JCI The Journal of Clinical Investigation

Distinct colitis-associated macrophages drive NOD2-dependent bacterial sensing and gut homeostasis

Gajanan D. Katkar, … , Saptarshi Sinha, Pradipta Ghosh

J Clin Invest. 2025. https://doi.org/10.1172/JCI190851.

Research In-Press Preview Gastroenterology Immunology Microbiology

Graphical abstract

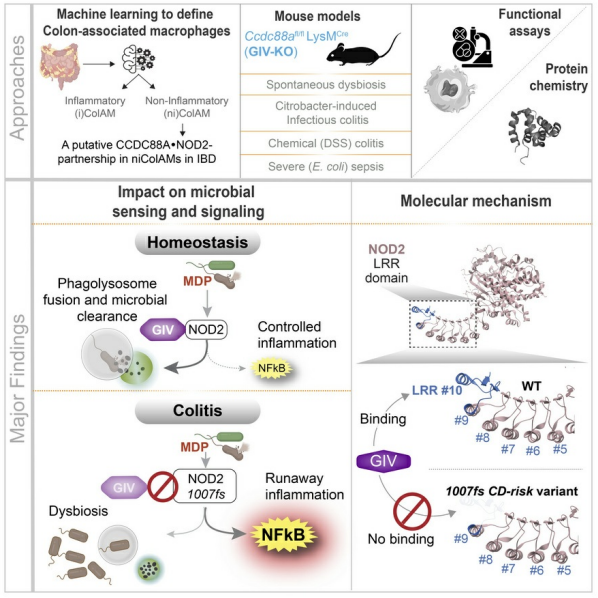

Find the latest version:

https://jci.me/190851/pdf

Distinct Colitis-Associated Macrophages Drive NOD2-Dependent Bacterial Sensing and Gut Homeostasis

Authors: Gajanan D. Katkar[1†], Mahitha Shree Anandachar[1,2†], Stella-Rita Ibeawuchi[2], Ella McLaren[1], Megan Estanol[1], Kennith Carpio-Perkins[1], Shu-Ting Hsu[1], Celia R. Espinoza[1], Jane Coates[1], Yashaswat S. Malhotra[1], Madhubanti Mullick[1], Vanessa Castillo[1], Daniella T. Vo[3], Saptarshi Sinha[1], and Pradipta Ghosh[1,4*]

Affiliations:
[1]Department of Cellular and Molecular Medicine, University of California San Diego, CA, USA.
[2]Department of Pathology, University of California San Diego, CA, USA.
[3]Department of Pediatrics, University of California San Diego, CA, USA.
[4]Department of Medicine, University of California San Diego, CA, USA.

[†] Equal contribution

Conflict of interest statement: The authors have declared that no conflict of interest exists.

KEY WORDS: GIV/Girdin, Guanine-nucleotide exchange modulators (GEMs), CCDC88A, Macrophage, NOD2, MDP, Microbes, Innate immunity

***Correspondence to**:

Pradipta Ghosh, M.D.; Professor, Departments of Medicine, and Cellular and Molecular Medicine, University of California San Diego; 9500 Gilman Drive (MC 0651), George E. Palade Building, Rm 232, 239; La Jolla, CA 92093. Phone: 858-822-7633: Fax: 858-822-7636: Email: prghosh@ucsd.edu

ABSTRACT (200-words)

Single-cell studies have revealed that intestinal macrophages maintain gut homeostasis through the balanced actions of reactive (inflammatory) and tolerant (non-inflammatory) subpopulations. How such balance is impaired in inflammatory bowel diseases (IBD), including Crohn's disease (CD) and ulcerative colitis (UC), remains unresolved. Here, we define colon-specific macrophage states and reveal the critical role of *non*-*inflammatory* *colon*-*associated* *macrophages* (niColAMs) in IBD recovery. Through trans-scale analyses—integrating computational transcriptomics, proteomics, and *in vivo* interventional studies—we identified GIV (*CCDC88A*) as a key regulator of niColAMs. GIV emerged as the top-ranked gene in niColAMs that physically and functionally interacts with NOD2, an innate immune sensor implicated in CD and UC. Myeloid-specific GIV depletion exacerbates infectious colitis, prolongs disease, and abolishes the protective effects of the NOD2 ligand, muramyl dipeptide, in colitis and sepsis models. Mechanistically, GIV's C-terminus binds the terminal leucine-rich repeat (LRR#10) of NOD2 and is required for NOD2 to dampen inflammation and clear microbes. The CD-associated *1007fs* NOD2-variant, which lacks LRR#10, cannot bind GIV—providing critical insights into how this clinically relevant variant impairs microbial sensing and clearance. These findings illuminate a critical GIV-NOD2 axis essential for gut homeostasis and highlight its disruption as a driver of dysbiosis and inflammation in IBD.

INTRODUCTION

Intestinal macrophages are critical for gut development, immunity and repair (1). Single-cell studies have revealed that gut homeostasis relies on the dynamic interplay between two antagonistic macrophage subpopulations: inflammatory “accelerators” and non-inflammatory “brakes” (2, 3). An imbalance in these subpopulations can lead to uncontrolled gut inflammation, as observed in inflammatory bowel diseases (IBD) such as Crohn’s disease (CD) and ulcerative colitis (UC) (4, 5). However, precisely defining these subpopulations and understanding their roles in health and disease, and the molecular mechanisms that control the same, remain significant challenges (6).

Recent advances in artificial intelligence (AI) and machine learning-guided transcriptomics have addressed this challenge by enabling the analysis of diverse macrophage states across both bulk and single-cell datasets (3, 7-10). Among these approaches, Boolean implication networks have emerged as a robust method with a decade-long track record (7, 8, 11, 12) for identifying universally conserved gene expression patterns (or “invariants”). These patterns remain consistent despite the variability introduced by tissue heterogeneity, circadian rhythms, metabolic states, species diversity, perturbations, stimuli, and disease conditions (7, 8, 11, 12). Using this network approach on a dataset of pooled isolated monocytes/macrophages representing greatest possible diversity, we recently defined ‘*S*ignature of *Ma*crophage *R*eactivity and *T*olerance’ (SMaRT; see **Figure 1A,** Supplemental information 1) as a conserved 338-gene signature representing macrophage continuum states, across the physiologic and pathologic spectra of “reactivity" and "tolerance" (3). We showed that while the conventional M1/M2 classification fails to capture the diversity, plasticity, and continuum of macrophage states in tissue during homeostasis and disease, the SMaRT model-derived definitions remain robust and consistently outperform other emerging classification schemes across contexts (3).

Here we sought to refine the SMaRT model in the context of IBD. We hypothesized that these definitions would yield robust classification and functional insights into the colitic environment. First, we formally define two macrophage subpopulations in the colon: inflammatory (iColAMs) and non-inflammatory (niColAMs) ---both in health and IBD. We find that tolerant niColAMs are essential for dampening inflammation and resolving infections, making them critical for recovery from IBD. We subsequently identify a previously unappreciated yet consequential physical and functional coupling in IBD-associated niColAMs between the innate immune sensor nucleotide-binding oligomerization domain-containing protein 2 (NOD2) and GIV (Gα-interacting vesicle-associated protein, also known as Girdin). NOD2, also known as NLRC2,

belongs to the nucleotide-binding domain and leucine-rich repeat (NLR) family and functions as an intracellular pattern recognition receptor (PRR) for muramyl dipeptide (MDP) derived from pathogens. NOD2 coordinates bacterial clearance and confers immunity (4), all while mounting a controlled inflammatory program that involves the dampening of NF-κB (13) activity that is TLR2/4-dependent (14-18). GIV, on the other hand, is a multimodular signal transducer and the prototypical member of the non-receptor *G*uanine nucleotide *E*xchange *M*odulator (GEM (19)) family of proteins. Unlike the canonical GPCR/G protein pathway, in which G proteins engage exclusively with ligand-activated GPCRs, GEMs like GIV bind and modulate G protein activity downstream of a myriad of cell-surface receptors (20-22). Of relevance here, GIV is a ubiquitously expressed molecule that is highly expressed in immune cells such as macrophages and serves as a "brake" for the cell surface PRR, TLR4 and modulates macrophage inflammatory responses to LPS (22) and gut barrier integrity during aging (23), cancer (23) and in IBD (7), and it's gene (*CCDC88A*) has emerged as a key determinant of macrophage polarization in the SMaRT model (3). We demonstrate that GIV interacts dynamically with NOD2 to facilitate microbial sensing and clearance while also suppressing inflammation. This protective mechanism is disrupted in the most clinically significant IBD-associated NOD2 risk variant, highlighting its relevance to disease pathology. These insights shed new light on the molecular pathways underlying gut homeostasis and the progression of IBD, offering potential therapeutic avenues for restoring balance in macrophage subpopulations.

RESULTS

Identification of distinct subpopulations of colon-associated macrophages

To contextualize the SMaRT model (**Figure 1A,** Supplemental information 1) within the human gut, and specifically, in IBD, we refined it using the largest, high-quality, full-thickness colon tissue transcriptomic dataset available for IBD (GSE83687) (24)-- the only dataset of its kind. Because the original model was built using purified macrophages and monocytes from diverse tissues, we assumed that refinement using bulk RNA-seq data would preserve a subset of macrophage-specific genes from the SMaRT model that are most relevant to IBD. Briefly, we employed a machine learning-based classifier on 338 SMaRT signature genes (3) (Supplemental information 1) to identify the classification accuracy of each of the SMaRT signature genes on healthy vs IBD-affected colon tissues (**Figure 1B**). This allowed us to formally define ColAMs in health as those expressing a core set of 24 genes [2, that are expressed highly in reactive inflammatory (i) ColAMs; 22 that are expressed highly in tolerant non-inflammatory (ni)ColAMs; **Figure 1C**] and in IBD, as those expressing a distinct set of 53 genes (26, that are expressed highly in reactive iColAMs; 27, that are expressed highly in tolerant niColAMs; **Figure 1C**). It is noteworthy that the brakes and accelerators in health are distinct from IBD (**Figure 1C**, *see* Supplemental information 2). The ColAM genes had AUC values greater than 0.70 (**Figure 1B,** Supplemental information 2) in discriminating between healthy and IBD-affected colon tissues (including UC and CD, see Supplemental information 2). KEGG pathway enrichment analysis revealed that model refinement led to enrichment of colitis-relevant pathways— including Toll-like receptor, NOD2, and TNF signaling (compare **Figure 1, D** and **E;** see Supplemental information 2 for gene lists).

When we tested their ability to distinguish healthy from colitis samples, the 53-gene ColAM signature (used independently as 26-gene iColAMs and 27-gene niColAMs) performed consistently better than the original SMaRT model (3), in both human (H vs. UC/CD; **Figure 1F**) and murine (H vs. dextran sodium sulfate (DSS), a chemical colitogen; **Figure 1G**) datasets. Leveraging a high-quality murine dataset of DSS-induced acute and chronic colitis (25), we found that i/niColAMs may be indued in temporally distinct patterns; iColAMs were induced acutely and persisted throughout the various DSS models, whereas niColAMs were induced exclusively in chronic model in which injury was repetitive in the form of 2 cycles of DSS followed by 3 weeks of recovery/washout, which is believed to better recapitulate the relapsing-remitting nature of IBD, (**Figure 1G**).

NOD2 may functionally couple with CCDC88A in colitis-associated non-inflammatory ColAMs

NOD2, located on chromosome 16, remains the most replicated genetic association in IBD, with a mean allelic odds ratio of 3.1 across studies (26, 27), and a well-established, though mechanistically debated, role in IBD pathogenesis (4, 28-32). Persistent controversy surrounds how NOD2 functions and how its variants drive colitis in both UC and CD (32-36). Given the enrichment of NOD signaling in IBD-associated colonic macrophages (**Figure 1E**) we investigated NOD-centric cellular processes in i/niColAMs.

Overlaying i/niColAM gene clusters with a published NOD1/2 interactome, as determined by BioID Proximity-Dependent Biotin Identification; (37), we identified a single candidate interactor: GIV, encoded by *CCDC88A* (**Figure 1H**). Notably, *CCDC88A* is part of the niColAM gene signature, which emerges during the recovery phase of DSS-induced colitis (**Figure 1G**). Its expression correlates with *NOD2*—but not *NOD1*—across 21 independent cohorts (**Figure 1I**) and is elevated in intestinal macrophages from UC and CD patients compared to healthy controls (**Figure S1A**).

We next leveraged a genome-wide siRNA screen in HEK293T cells (38) that assessed MDP-induced hyperactivation of NFκB. While NOD2 variants are known to impair bacterial clearance and disrupt NFκB activation (13, 29, 38, 39), paradoxically, the gut mucosa of IBD patients often shows heightened NFκB activity (40-44). Loss-of-function NOD2 variants, such as the CD-associated *1007fs* (45), are also known to impact the severity of disease course in UC (46). Based on these observations, NOD2 is believed to restrict activation of the NFκB pathway by TLR2/4 (14-18) and its dysfunction causes runaway inflammation, thereby increasing the risk of colitis. Consistent with these observations, the functional-genomic screen revealed that among all i/niColAM-genes, depletion of *CCDC88A* within the niColAM cluster (genes presumed to be critical for reducing inflammation) emerged as the most consequential perturbation that increases NFkB activity (**Figure 1J**).

These findings suggest that CCDC88A may functionally couple with NOD2 to restrain inflammation in colonic macrophages, providing a strong rationale to investigate the protective niColAM state during colitis recovery.

GIV is required for MDP/NOD2-mediated bacterial clearance and controlled inflammation

Given its recently identified role in modulating macrophage responses (22), we asked if GIV may be a functional modulator of the cytosolic sensor, NOD2. To study the role of GIV in MDP/NOD2-induced

inflammatory responses in macrophage *in vitro*, we used 4 cell-based models: (i) GIV-depleted (shGIV) RAW 264.7 murine macrophage cells; this previously-validated cell model displays ~85-90% depletion of GIV protein by immunoblotting (22) (**Figure 2A**)]; (ii) THP1 NFkB-SEAP reporter human macrophage lines depleted or not of >~90% GIV protein (by CRISPR; **Figure 2D**). (iii) thioglycolate-induced murine peritoneal macrophages (TGPMs) isolated from myeloid-specific conditional GIV knockout (GIV-KO) mouse, generated previously (22) by crossing Girdin floxed mice to *LysM*cre mice, and confirmed to have ~85-90% depletion of GIV protein; and (iv) THP1 human macrophage lines depleted or not of >~90% GIV protein (by CRISPR; **Figure 2J**).

In GIV-depleted RAW macrophages, MDP/NOD2-induced NFκB activity was significantly elevated (**Figure 2, B and C**), as determined by luciferase reporter assays. Dynamic NFκB reporter assays in THP1 reporter cells further confirmed the findings, adding robustness to the results (**Figure 2, E-G**). These findings were corroborated in HeLa cells (**Figure S1, B-D**), a cell line commonly used to study NOD2-dependent processes in plasmid transfection settings (47, 48). Briefly, compared to control cells, GIV-depleted HeLa cells (by CRISPR; **Figure S1B**) showed significantly higher MDP/NOD2-induced NFkB activity, confirming the role of GIV in dampening NFkB activity. Consistent with its role in dampening inflammation, GIV depletion in TGPMs led to a ~3-4-fold increase in proinflammatory cytokines [interleukin (IL)1β, IL6, and tumor necrosis factor (TNF)α], as measured by ELISA (**Figure S1, E and F**). Hyper-induction of proinflammatory cytokines was accompanied by a concomitant suppression of the anti-inflammatory cytokine, IL10 (**Figure S1, E and F**). These cytokine profiles were consistent with gene expression patterns assessed via qPCR (**Figure S1G**).

When TGPMs were infected with *a*dherent-*i*nvasive *E*scherichia *c*oli strain-LF82 (*AIEC*-LF82), isolated from CD patients (49), GIV-KO TGPMs exhibited delayed bacterial clearance compared to WT controls (**Figure 2, H and I**). Similarly, GIV-KO THP1 cells reproduced these findings (**Figure 2, K and L**). Immunofluorescence imaging further confirmed that GIV-KO TGPMs retained significantly higher numbers of pathogenic *AIEC*-LF82 bacteria (**Figure 2M)**.

Tandem mass tag (TMT)-based quantitative proteomics of GIV-depleted RAW macrophages revealed distinct proteomic differences after 16 hours of MDP stimulation (**Figure 2N**). While control cells activated robust NOD2-dependent signalling and inflammasome assembly (**Figure 2O**), GIV-depleted cells showed an acute-phase response and heightened expression of proinflammatory cytokines (**Figure 2P**).

Together, these results identify GIV as a critical mediator of MDP/NOD2 signaling. GIV is essential for maintaining a balanced pro- and anti-inflammatory cytokine response and promoting effective bacterial

clearance. In its absence, macrophages exhibit exaggerated NFκB-driven inflammation but fail to clear bacteria efficiently (**Figure 2, Q-R**), suggesting that GIV's role in microbial clearance may be independent of its modulation of NFκB signaling.

GIV is required for phagolysosomal fusion

To understand why GIV-deficient macrophages retain higher intracellular bacterial loads despite heightened NFκB activity (**Figure 2R**), we next investigated whether GIV plays a direct, NFκB-independent role in bacterial clearance. Because NOD2-dependent response to degraded bacteria requires the phagosomal membrane potential and the activity of lysosomal proteases (50), we hypothesized that GIV may facilitate phagolysosomal fusion.

We used two complementary approaches to test this. First, we challenged TGPMs in vitro with *AIEC*-LF82 and assessed the spatial proximity of internalized bacteria to LAMP1-positive lysosomes by confocal immunofluorescence microscopy (**Figure 3A**). In control (WT) cells, *AIEC*-LF82 bacteria were frequently found near LAMP1-positive structures (**Figure 3B**), suggesting efficient delivery of phagosomes to lysosomes. By contrast, GIV-deficient macrophages showed a marked reduction in bacteria-lysosome proximity (**Figure 3B**), suggesting disrupted lysosomal targeting.

Second, we used quantitative transmission electron microscopy (TEM) to visualize phagolysosomal fusion events and quantify bacterial burden over time (**Figure 3C**). GIV-deficient macrophages harbored visibly higher numbers of intracellular *AIEC*-LF82 compared to WT controls (**Figure 3D**), both at 5- and 30-minutes post-infection (**Figure 3E**), confirming impaired bacterial clearance. TEM imaging also revealed stark ultrastructural differences: while WT cells exhibited numerous phagolysosomal (PL) fusion events (**Figure 3F**, arrowheads). GIV-deficient macrophages showed markedly fewer fusion events (**Figure 3G**), and retained a higher number of unfused lysosomes (**Figure 3H**), suggesting a defect in phagosome maturation and lysosome engagement, but not lysosome biogenesis.

These findings define a mechanistically distinct, NFκB-independent role for GIV in promoting phagolysosomal fusion. In its absence, bacterial clearance fails despite heightened inflammatory signaling, underscoring GIV's dual function: restraining inflammation via NFκB modulation and promoting pathogen elimination through lysosomal trafficking (**Figure 3, I-J**).

GIV-KO mice develop dysbiosis and exacerbated and protracted *Citrobacter*-induced colitis

To investigate the role of GIV in vivo, we employed a myeloid-specific GIV-KO (*Ccdc88a*$^{fl/fl}$/*LysM*^{Cre}) model (see *Methods*) (22). We found that these mice spontaneously develop dysbiosis by ~8-12 wk (**Figure 4, A and B**; **Figure S2**). Notably, the strain *Rhizobiales* —uniquely associated with CD patients and absent in healthy controls (P = 0.037) (51) —detected in 100% of GIV-KO mice (5/5) but was undetectable in control littermates (**Figure 4, A and B**; **Figure S2**).

Upon *Citrobacter* challenge (**Figure 4C**), GIV-KO mice exhibited an increased acute fecal bacterial load (**Figure 4D**; 1st wk) and an abnormal delay in bacterial clearance, leading to chronic infection (**Figure 4D**; 7th wk). These mice also demonstrated hallmark features of chronic colitis, including colon shortening (**Figure 4E**), patchy transmural inflammation affecting the small intestine, colon, and rectum (**Figure 4, F and G**), as well as focal muscle hypertrophy and collagen deposition (**Figure 4, H and I**). Because the absolute numbers of macrophages and specifically, M2 macrophages—defined by established conventional markers CD68 and CD163, respectively (52-54)—were comparable between *Citrobacter*-infected control and GIV-KO intestinal tissues (**Figure S3, A-D**), we conclude that GIV deficiency impairs the healing functions of ColAMs without affecting macrophage trafficking or polarity-defining M2 markers at the site of infection.

Collectively, these findings highlight a critical role of GIV in bacterial clearance and the resolution of inflammation. Its absence promotes dysbiosis and chronic infectious colitis, underscoring GIV's essential role in maintaining intestinal immune homeostasis.

Protective MDP/NOD2 signaling is abolished in myeloid specific GIV-KO mice.

Prior studies have shown that pre-treatment with MDP ameliorates infection/bacteremia (55, 56), fatality in sepsis (57) and chemical (e.g., trinitrobenzene sulfonic acid, TNBS and DSS)-induced colitis (15); we asked if these protective actions of MDP require GIV. Compared to WT controls, we found that the GIV-KO mice developed significantly worse DSS-induced acute colitis (**Figure 5A**), as determined by disease activity index (**Figure 5, B and C**) and histological composite scores accounting for deformation of colon crypts and increased immune infiltration in the colon (**Figure 5, D and E**) and; the latter is a composite score of stool consistency, weight loss and the presence of fecal blood (22, 58, 59). Pre-treatment with MDP ameliorated the severity of colitis in WT, but not GIV-KO mice (**Figure 5, B-E**). Because the absolute numbers of CD68+ve M1 and CD163+ve M2 macrophages were comparable between control and GIV-KO DSS-exposed intestinal tissues (**Figure S3E-H**), GIV deficiency appears to impact MDP-induced ColAM properties without affecting macrophage trafficking or polarity-defining M2 markers at the site of inflammation.

Similar results were observed in the case of *E. coli*-induced sepsis (**Figure 5F**); fatality was higher in GIV-KO mice compared to WT controls (**Figure 5G**). Pre-treatment with MDP reduced fatality in WT, but not GIV-KO mice (**Figure 5G**). These findings demonstrate that GIV is required for the protective MDP/NOD2 signaling in the setting of infection/inflammation.

Prior studies have shown that MDP priming of NOD2 protects cells from excessive inflammation induced by lipopolysaccharide (LPS) (15, 60). To determine if this protective effect requires GIV, we used GIV-depleted (shGIV) RAW 264.7 murine macrophages and WT controls (shC) to assess NFκB activation following LPS stimulation, with or without MDP pretreatment. In WT cells, MDP pretreatment significantly reduced NFκB activation, but this protective effect was markedly compromised in GIV-depleted cells (**Figure 5H**). The findings were also reproduced in CRISPR-depleted human THP-1 cells expressing an NFκB activity-tracking reporter, enabling continuous monitoring of signaling dynamics. The presence of GIV was required for sustained suppression of NFκB activity, evident as early as 6 h and maintained through 24 h (**Figure 5I**). Similar findings were observed in HeLa cells, which express the MD2 co-receptor essential for LPS/TLR4 signaling (48, 61-65) , albeit at low levels (66). In control HeLa cells, MDP pretreatment reduced NFκB activation significantly, both with endogenous NOD2 (**Figure S1H**) and exogenously overexpressed NOD2 (**Figure S1I**). In cells without GIV, this protective effect was either diminished (**Figure S1H**) or virtually abolished (**Figure S1I**). Additionally, when MDP-primed TGPMs were infected with the pathogenic *AIEC*-LF82 strain (49), MDP treatment accelerated bacterial clearance in WT cells but not in KO TGPMs (**Figure 5, J-L**).

These findings demonstrate that GIV is essential for protective MDP/NOD2 signaling, which counteracts LPS/TLR4-driven proinflammatory NFκB signaling (**Figure 5M**). Without GIV, NFκB signaling becomes excessive, and bacterial clearance is delayed and impaired (**Figure 5N**).

MDP/NOD2 signals induce niColAMs and GIV is required for such induction

To assess the role of MDP/NOD2 signaling in modulating colonic i/niColAM populations, we analyzed publicly available transcriptomic datasets of DSS-induced colitis spanning acute, chronic, and recovery phases (**Figure 6A**), using composite gene signatures of i/niColAM subsets. iColAMs were elevated during the acute phase but declined during the chronic and recovery phases (**Figure 6B**), while niColAMs showed the opposite trend—increased abundance during recovery (**Figure 6B**).

Because GIV is required for the protective effects of MDP/NOD2 signaling in DSS-induced colitis (**Figure 5, A-E**), we next asked whether this protection arises from MDP's ability to promote early induction of ni-ColAMs, thereby accelerating recovery from acute colitis. We analyzed colon transcriptomes from WT and GIV-KO mice treated with DSS-colitis, with or without MDP treatment (**Figure 6C**). In WT mice, a composite niColAM score robustly distinguished MDP-treated WT colon tissues from untreated WT controls (classification accuracy = 1; **Figure 6D**). This indicates early upregulation of healing niColAMs by MDP—earlier than anticipated from phase-specific trends (**Figure 6B**)—and potentially accelerating recovery. By contrast, in GIV-KO mice, MDP treatment elevated iColAM scores (also with classification accuracy = 1; **Figure 6D**), consistent with the observed exacerbation of inflammatory responses (**Figure 5, A-E**). Gene Ontology (GO) analysis of differentially expressed genes corroborated these findings, revealing activation of protective and reparative programs in MDP-treated WT mice, but not in GIV-KO mice (**Figure 6, F-I**; see **Supplemental information 3** for full genes list).

To determine whether the healing niColAM population aligns with conventional non-inflammatory macrophage (M2) populations, we performed bulk RNA-seq deconvolution. This revealed a close transcriptional resemblance between niColAMs and M2-like (anti-inflammatory) macrophages, which were enriched in MDP-treated WT, but not GIV-KO, mice (**Figure 6, J-K**).

Together, these results underscore the essential role of GIV in enabling MDP/NOD2-mediated protection in vivo—by selectively promoting the emergence of healing niColAMs that counterbalance pro-inflammatory iColAMs and restore tissue homeostasis.

The GIV●NOD2 interaction is direct and dynamically regulated by MDP

NOD2 typically exists in an inactive, ADP-bound conformation stabilized by intramolecular interactions (67, 68). Upon binding its ligand, MDP, NOD2 undergoes conformational changes that facilitate ADP-to-ATP exchange, self-oligomerization, and downstream signaling (67, 68) (**Figure 7A**).

To determine whether GIV physically interacts with NOD2, we performed co-immunoprecipitation experiments and found that full-length, endogenous GIV and NOD2 form complexes in THP1-derived macrophages (**Figure 7B**). *In situ* proximity ligation assay (PLA) using antibodies against the native proteins confirmed this interaction and revealed that the abundance of GIV●NOD2 complexes is enhanced by MDP stimulation, peaking around 1 hour post-treatment (**Figure 7, C-E**). Co-immunoprecipitation assays using exogenously expressed, epitope-tagged GIV and NOD2 proteins further validated this interaction and its

ligand-dependent dynamic regulation. Whether GIV-FLAG or HA-NOD2 was used as bait, assembled GIV●NOD2 complexes were detected in immune complexes within ~1-3 h post-MDP stimulation, and declined by ~6 h (**Figure 7, F-G, Figure S4A**), underscoring the temporally regulated nature of the interaction.

To visualize the ultrastructural context of GIV●NOD2 complex assembly, we performed immunogold electron microscopy on TGPMs 1 h after MDP stimulation. Using 18 nm and 12 nm gold-conjugated antibodies against GIV and NOD2, respectively, we observed NOD2 colocalizing with membrane-associated GIV, predominantly along actin filaments (**Figure 7, H-L**) within particle-rich cytoplasmic structures (69) (PaCS; which contain polyubiquitinated proteins and proteasomes) (**Figure 7, H and J**) and around swollen, morphologically abnormal mitochondria (**Figure 7M**).

Together, these findings demonstrate that the GIV●NOD2 interaction is both direct and dynamically regulated by MDP. The complex associates with the membrane and cytoskeletal elements, supporting its potential role in NOD2-mediated signaling and cellular responses (70).

The C-terminus of GIV directly binds the LRR domain of NOD2

GIV is a large, multimodular scaffold protein (1871 amino acids) with several defined interaction domains (**Figure 8A**). NOD2, in contrast, contains three major domains: CARD, NBD, and LRR (**Figure 8B**). While NOD1 and NOD2 share structural similarities, co-immunoprecipitation analyses revealed that GIV specifically binds to NOD2 but not NOD1 (**Figure 8C**), indicating that the GIV●NOD2 interaction is selective.

Given that the ~210 amino acid C-terminal (CT) module of GIV mediates interactions with a variety of receptors and sensors via short linear motifs (SLIMs) (**Figure 8A**), we tested whether this region was sufficient for NOD2 binding. Indeed, GIV-CT bound NOD2 (**Figure S4B**) but did not interact with NOD1 (**Figure S4B**), further confirming specificity.

To identify the domain of NOD2 responsible for GIV binding, we performed co-immunoprecipitation assays using NOD2 deletion mutants lacking the CARD domains (ΔCARD), NBD (ΔNBD), or LRR (ΔLRR) domains (**Figure 8, E and F**). These studies showed that GIV binding was independent of the CARD and NBD domains and instead required the LRR domain (**Figure 8, E and F**). Notably, deletion of the terminal repeat in the LRR domain (ΔLRR10) virtually abolished GIV binding (**Figure 8, G and H**). These findings were corroborated by co-immunoprecipitation using full-length proteins (**Figure S4E**) and GST-pulldown studies using GIV-CT (**Figure 8I**, **Figure S4F**). Moreover, site-directed mutagenesis of key arginine residues

in NOD2 (R1034 and R1037) (**Figure 8D)**, which stabilize its terminal LRR (**Figure 8H)**, reduced GIV binding (**Figure 8I**).

Together, these results demonstrate that the terminal LRR repeat of NOD2 is essential for its interaction with the C-terminal region of GIV, providing insights into the molecular basis of their functional coupling (**Figure 8G-I**).

GIV fails to bind the CD-associated NOD2 *1007fs* variant, which lacks the terminal LRR

We next examined whether GIV binding is altered by CD-associated NOD2 variants (*R702W*, *G908R* and *1007fs*) which collectively account for ~80% of mutations associated with CD susceptibility (**Figure 9A**) (32, 71). These mutations affect residues located within or near the LRR domain (**Figure 9B**). Co-immunoprecipitation assays revealed that two variants, R702W and 1007fs (**Figure 9C**), did not bind to the C-terminal region of GIV. Notably, these variants are associated with high disease penetrance (~100%; **Supplementary Table 1**). By contrast, the G908R variant—which disrupts the MDP-binding interface (72, 73)—retained GIV binding comparable to NOD2-WT (**Figure 9C**). Further studies confirmed that the *1007fs* variant remained incapable of binding GIV even upon MDP stimulation (**Figure 9D**).

To assess the functional consequences of these binding defects, we examined how the CD-risk variants modulate NFκB signaling in response to LPS following MDP priming. In luciferase reporter assays, MDP pretreatment significantly suppressed LPS-induced NFκB activation in the presence of NOD2-WT (**Figure 9, E and F**), conferring 65% protection. However, this protective effect was reduced in cells expressing the NOD2 variants (**Figure 9F**; red *p*-values). For instance, while NOD2-WT conferred ~65% protection, the NOD2-*1007fs* variant (~20% protection) or other GIV-binding deficient mutants (**Figure 9F**; red p values). In GIV-KO cells, suppression by NOD2-WT dropped from ~65% to ~10%, further confirming the role of GIV in this protective response (**Figure 9F**; gray *p*-values). The residual ~10–20% suppression observed in conditions lacking GIV●NOD2 coupling (e.g., with NOD2-1007fs or in GIV-KO cells) suggests minor contributions from GIV-independent mechanisms or a consequence of endogenous NOD2.

To investigate the impact of GIV on NOD2-dependent microbial clearance, we performed gentamicin protection assays in THP1-derived macrophages transfected with either NOD2-WT or the 1007fs variant, followed by infection with adherent-invasive E. coli (*AIEC*-LF82) (**Figure 9, G and H**). Macrophages expressing NOD2-WT efficiently cleared bacteria, whereas those with the 1007fs variant showed impaired clearance, reflected by elevated intracellular bacterial burden. Notably, GIV-KO macrophages expressing

NOD2-WT displayed a defect similar to GIV proficient control macrophages expressing the NOD2 1007fs variant (**Figure 9I**). These findings indicate that both GIV and the terminal LRR domain of NOD2 (GIV-binding site on NOD2) are critical for effective NOD2-mediated bacterial clearance.

Collectively, these findings highlight the critical role of the GIV●NOD2 interaction in mediating the protective effects of MDP signaling. Disruption of this interaction—such as in patients harboring the 1007fs CD-risk variant—may contribute to exaggerated inflammatory responses (via impaired suppression of LPS-induced NFκB activation) and hinder microbial clearance and restoration of intestinal homeostasis (**Figure 9, J and K)**.

DISCUSSION

Our study presents three major findings: First, we identified a core gene signature that formally defines colon-associated inflammatory and non-inflammatory macrophage states, in both health and IBD. Within this signature, we established GIV (*CCDC88A* gene) as a critical physical and functional interactor of NOD2, enabling protective and homeostatic NOD2 signaling specifically in non-inflammatory macrophage. This protective mechanism GIV●NOD2 axis operates within the lamina propria across models of acute colitis (DSS-induced), chronic inflammation (IBD), and acute systemic infection (sepsis). Third, we delineated the molecular basis of the GIV–NOD2 interaction, showing that it is direct, dynamic, and essential for dual antimicrobial and anti-inflammatory macrophage responses to bacterial sensing (**Figure 9, J and K**). Specifically, this interaction (i) dampens NFκB-dependent inflammatory signals, and (ii) enhances NFκB-independent pathways that drive phagolysosomal fusion and bacterial clearance. Together, these dual functions prevent excessive inflammation while ensuring effective microbial control.

Importantly, our findings also reveal a molecular mechanism for the pathogenicity of the high-penetrance CD-associated NOD2 variant, 1007fs. In the dysbiotic colitic gut, where NOD2 is essential for regulating inflammation and microbial clearance, the inability of GIV to bind the truncated NOD2-*1007fs* variant provides mechanistic insight into how this risk allele contributes to persistent inflammation, dysbiosis and mucosal pathology. These insights redefine the molecular logic of innate immune sensing and signal integration through NOD2 in intestinal macrophages

ColAM Signatures Provide a Computational Framework to Map Macrophage States in the Gut.

Our machine learning–assisted analyses identified a subset of genes—ColAMs—from a broader macrophage activation signature (SMaRT; 338 genes), which reliably distinguish inflammatory (iColAM) from non-inflammatory (niColAM) macrophages in colon tissue. The ColAM signature, particularly its 53-gene IBD-associated subset, is clinically relevant and reflects dynamic, disease-relevant macrophage states in transcriptomic datasets.

Notably, our findings show that IBD-ColAMs enrich for gut-relevant pathways and successfully resolved macrophage functional states even in bulk RNA-seq datasets, attesting to their robustness and specificity. In fact, we show that i/niColAMs dynamically reflect shifts in macrophage function that track with colitis severity—something conventional markers (like CD163) fail to do.

In healthy tissue, niColAMs predominate, likely reflecting the need for tolerogenic surveillance in a microbe-rich environment protected by a single epithelial layer. These macrophages may act as “brakes”—providing low-grade, tolerogenic surveillance that protects epithelial stem cells and neurons from collateral damage. In contrast, during chronic inflammation and dysbiosis, iColAMs act as “accelerators,” while niColAMs act as “brakes” to restrain runaway inflammation. The niColAMs in the setting of colitis appear to transcriptionally resemble M2 macrophages, which have been implicated in mounting an adequate healing response. The niColAMs are induced by NOD2 activation and GIV appears to be essential for such induction. Disruption of this balance—whether through hyperactive iColAMs or impaired niColAMs (as seen in GIV KO mice)—may perpetuate inflammation and disease. This “brake and accelerator” framework offers a new conceptual framework for understanding macrophage regulation at mucosal barriers and presents a foundation for therapeutic targeting of macrophage states in IBD.

GIV Enables NOD2 to Restrain NFκB-Driven Inflammation in Non-Inflammatory Macrophages

Among the 53 IBD-ColAM genes, *CCDC88A* (GIV) emerges as the sole candidate that both physically and functionally interacts with NOD2. While NOD2’s suppression of NFκB-driven inflammation is well recognized but poorly understood (13), we now show that GIV is essential for this protective function. GIV physically interacts with NOD2, and such binding enables NOD2 to (i) suppress excessive NFκB activity and (ii) drive bacterial clearance via cytoskeletal and phagolysosomal pathways—both essential for mucosal immunity and homeostasis. In the absence of GIV, NOD2's antimicrobial and anti-inflammatory functions are impaired, macrophages adopt a reactive phenotype, and host defenses falter. Consequently, macrophages adopt reactive phenotypes, display impaired microbial control, and the host shows heightened susceptibility to colitis and sepsis. Notably, GIV’s inability to bind the NOD2-1007fs variant supports a molecular mechanism linking GIV to chronic intestinal inflammation. These data position GIV as a central integrator of gut immune regulation and tissue repair.

These findings build on prior work showing GIV acts as a “brake” within the LPS/TLR4 signaling cascade (22). GIV's conserved C-terminal motif binds and dampens inflammatory signaling by TLR1/2, TLR2/6, and TLR3, inducing tolerogenic programs aimed at homeostasis and immunity (22). Thus, GIV emerges as a point of convergence for major pattern recognition receptors (PRRs), coordinating tolerogenic responses during microbial sensing (22, 37, 74).

GIV Couples NOD2 to Other NFkB-independent Signaling Domains and Organelle Functions

Our mechanistic analyses show that GIV binds NOD2 via its C-terminal 210 amino acids, interacting specifically with the terminal LRR repeat of NOD2. This identifies GIV as only the third known protein to directly engage the NOD2-LRR region (75), and one of very few to do so in a way that enhances NOD2's protective, NFκB-suppressive signaling. While our study defines how GIV shapes NOD2 function, the possibility of reciprocal regulation remains unexplored. It is possible that the GIV●NOD2 interaction may collaborate or compete with GIV-dependent cAMP inhibition (via Gi activation and Gs inhibition) (76), or temporally-spatially cross-regulate each other, impacting myriad of inflammatory signals that are shaped by cAMP flux (77-79), including phagolysosomal fusion events that are critical for microbial clearance (80). This would position NOD2 as another receptor modulating trimeric G-proteins and cAMP through GIV's C-terminal SLIM motifs, joining a lengthy list of priors (81). Future studies will identify the specific SLIM mediating this interaction and investigate overlap with motifs for TLR4 or Gαi/s binding.

Taken together with its impact on NFkB-driven inflammation, the NOD2-GIV module likely evolved to balance pathogen elimination with inflammatory restraint. This dual functionality—dampening NF-κB while ensuring efficient phagolysosomal fusion—may be key to preventing collateral tissue damage during infection and preserving mucosal homeostasis.

The Loss of GIV●NOD2 Interaction Defines the Functional Defect in the 1007fs CD-Associated Variant

Among the three main CD-associated variants (*R702W*, *G908R*, and *1007fs*) that interfere with bacterial recognition (82), G908R's defect lies in impaired MDP contact (72, 73) whereas R702W and 1007fs show defects in palmitoylation and PM localization (37). Only the *1007fs* variant, which lacks the terminal LRR repeat, fails to regain functionality upon restoring PM localization (83), indicating that *1007fs* variant lacks key functions, perhaps because of the truncated terminal LRR repeat. We show that the *1007fs* variant does not bind GIV and that it lacks the same terminal LRR repeat that is essential for the NOD2●GIV interaction. Because our conclusions are supported by both co-immunoprecipitation and *in vitro* pulldown assays using recombinant NOD2-LRR proteins, it unlikely that mislocalization artifacts explain the binding loss [as proposed for other NOD2 interactors, e.g., Erbin (84)]. Thus, GIV emerges as a first-in-class NOD2-interactor that specifically requires the terminal (10^{th}) LRR repeat —precisely the region lost in the 1007fs variant. The

observation that NOD2-1007fs–expressing cells phenocopy GIV-deficient cells, exhibiting heightened inflammation and impaired microbial clearance, further underscores the critical role of this terminal repeat as the GIV-binding site, whose loss disrupts NOD2's protective signaling.

Because this variant (also termed *3020insC*) is most consistently associated with CD across multiple studies and population groups, and displays 100% disease penetrance, it is not surprising that our GIV-KO animals challenged with *Citrobacter* develop key features of CD : patchy ileocolitis, transmural inflammation, focal muscle hypertrophy, fibrosis, and dysbiosis. Notably, these features arise within just 7 wks — substantially earlier than the only other known spontaneous murine model of CD SAMP1/YitFcs, which takes ~30 wks (85). Future studies will explore whether GIV-KO mice recapitulate the full molecular and phenotypic spectrum of Crohn's disease, including defective innate/adaptive immunity and fistula formation.

LIMITATIONS OF STUDY

Although our conclusions are grounded in NOD2-specific phenotypes elicited by MDP stimulation, we lacked tools to directly interrogate the GIV●NOD2 interaction in vivo. Future studies will require engineered mutants of GIV and NOD2 that selectively disrupt binding, enabling direct assessment of interaction-dependent functions. Additionally, the observation that MDP enhances GIV●NOD2 binding raises the possibility that other variables—such as pH, ATP levels, or subcellular localization—may modulate this interaction. These contextual factors, known to influence the NOD2 interactome, were not investigated in this study but remain important avenues for future exploration. Finally, we know that GIV can modulate signaling downstream of multiple TLRs, and NOD2 can suppress a subset of those TLRs (15, 17, 22, 86). While this study establishes the role of a functional coupling between GIV and NOD2 in dampening TLR4-driven inflammation, further studies are needed to determine whether GIV-dependent NOD2 signaling broadly suppresses TLR-mediated responses beyond TLR4.

METHODS

Sex as a biological variable

All animal experiments used male mice, as this study did not assess sex as a biological variable. Male mice were prioritized to ensure continuity with prior sepsis and colitis studies on NOD2 biology. Since neither Crohn's disease nor the NOD2 1007fs variant shows sex-based susceptibility, and both GIV and NOD2 functions are established across sexes, the core molecular mechanisms are expected to apply broadly.

Statistics

All experimental values are presented as the means of replicate experiments ± SEM. Statistical analyses were performed using Prism 9 (GraphPad Software). Differences between the two groups were evaluated using AUC classification accuracy, two-tailed Student's t-test (parametric) and Mantel-Cox log rank test. To compare more than three groups, the unpaired multiple t-test, one-way or two-way analysis of variance with Tukey's multiple comparisons testing was used. p-value < 0.05 were considered significant.

Study approval

All mice studies were approved by the University of California, San Diego Institutional Animal Care and Use Committee (IACUC) under protocol number S17223.

Data availability

The code related to the computational analyses used in this paper is available at: https://github.com/sinha7290/NOD2. Mass spectrometry proteomics data have been deposited in the ProteomeXchange Consortium via the PRIDE (87) partner repository under the dataset identifier PXD066180. Newly generated transcriptomic datasets reported in this paper have been deposited in NCBI's Gene Expression Omnibus under the dataset identifier GSE299285. All other publicly available transcriptomics datasets are accessible through NCBI's Gene Expression Omnibus database. All data supporting the findings of this study are included in the Supporting Data Values file, and complete, unedited blots are in the supplemental material.

Author contributions

G.D.K, M.A and P. G. conceptualized the project. G.D.K., M.A., S.S, ME, EM, K.C-P, S-T.H, J.C, Y.M, C.R.E, M.M and V.C, were involved in data curation and formal analysis. D.T.V. carried out 16S microbiome analysis. S.S, with supervision from P.G, carried out all the transcriptomic and proteomic analyses. G.D.K conducted all animal studies. M.A conducted all biochemical studies. V.C assisted G.D.K. for ELISA. Y.M assisted G.D.K. for qPCR and image analyses. C.R.E and S-R.I performed all molecular biology tasks (construct design, cloning and mutagenesis). G.D.K. and P.G. prepared Figures for data visualization. P.G. wrote the original draft; all authors reviewed and edited the manuscript. P.G. supervised and acquired funding to support the study. All co-authors approved the final version of the manuscript.

Acknowledgments

This work was supported by the National Institutes of Health (NIH) grant (R01-AI141630, UG3TR003355, UG3TR002968, and R01-AI55696), a pilot award from the Propel a Cure Foundation and the Leona M. and Harry B. Helmsley Charitable Trust (to P.G.). G.D.K. received support from the American Association of Immunologists Intersect Fellowship Program for Computational Scientists and Immunologists and the American Heart Association Career Development Award (24CDA1268506). M.S.A. was supported by an American Heart Association Predoctoral Fellowship (25PRE1357971). S.S. was supported by The AAI Intersect Fellowship Program. Additional support includes T32GM8806 (to D.V.). S.-R.I. received a postdoctoral fellowship from the NIH (3R01DK107585-02S1), and M.M. was supported by a UC San Diego Agilent Center of Excellence Postdoctoral Fellowship. The authors thank the UC San Diego Cellular and Molecular Medicine Electron Microscopy Core (RRID: SCR_022039) for access to equipment and technical assistance; the Core is partially supported by NIH grant S10-OD023527. Data in this manuscript were generated at the UC San Diego Institute of Genomic Medicine using an Illumina NovaSeq 6000, funded by NIH SIG grant S10-OD026929. The authors acknowledge instrumentation resources at the UC San Diego Agilent Center of Excellence in Cellular Intelligence. The content is solely the authors' responsibility and does not necessarily represent the official views of the Helmsley Charitable Trust or the NIH.

FIGURES AND LEGENDS

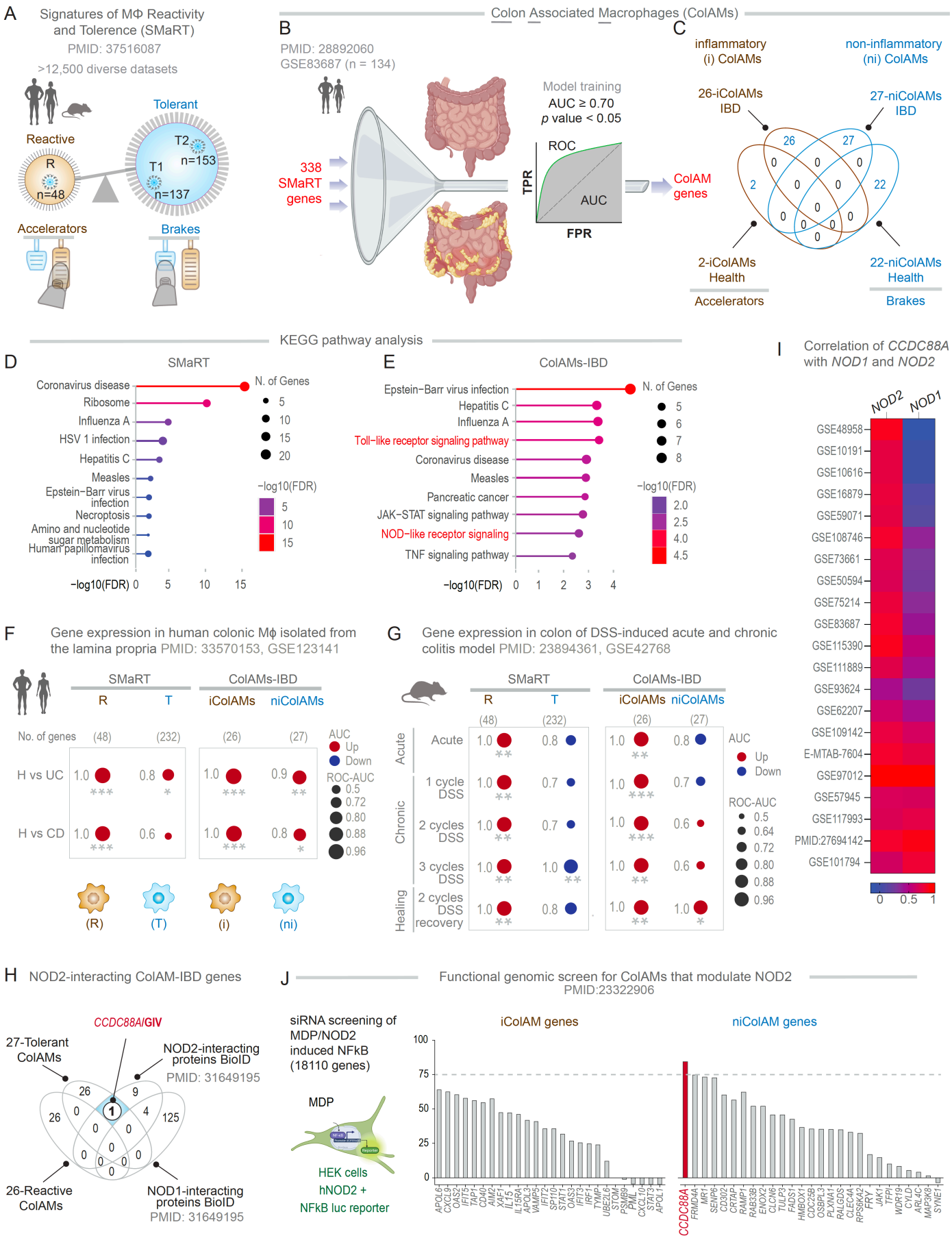

Figure 1. Identification of *CCDC88A* as a putative NOD2-modulator in IBD-associated macrophages.

A. Key steps of the previously published workflow (3) used to develop the computational model of macrophage continuum states—*S*ignatures of *Ma*crophage *R*eactivity and *T*olerance (SMaRT)—are shown. SMaRT identifies invariant gene clusters representing reactive (R) and tolerant (T1, T2) states across over 12,500 diverse transcriptomic datasets. The schematic below illustrates their opposing roles: reactive macrophages act as "accelerators," while tolerant states serve as "brakes," working antagonistically to fine-tune inflammatory responses to perceived threats.

B. Key steps used here to refine SMaRT in the context of the gut mucosa and derive colon-associated macrophage signatures (ColAMs) using a dataset (GSE83687) (24) comprised of both healthy and IBD samples. SMaRT genes were trained to derive a subset of ColAMs that could classify healthy vs IBD sample, achieving an area under the curve ≥ 0.7 and *p*-value ≤ 0.05 (Fisher's Exact test).

C. Inflammatory and non-inflammatory ColAM-defining genes identified here, in health and IBD.

D-E. KEGG pathway enrichment analysis for SMaRT (**D**) and the ColAM-IBD (**E**) gene sets.

F-G. Bubble plot showing ROC-AUC (circle size) and regulation (red = up, blue = down) for classifying healthy vs. CD and healthy vs. UC in human colonic lamina propria (GSE123141) (**F**) and DSS-induced acute, chronic and healing phase of murine colitis models (**G**). This classification is based on macrophage gene signatures of reactivity 'R' and tolerance 'T', identified in the SMaRT model and the i/niColAMs, used independently. Welch's two-sample unpaired t-test is applied to the composite gene signature score to compute p-values (* $p \leq 0.05$; ** $p \leq 0.01$; *** $p \leq 0.001$).

H. Venn diagram of ColAM genes identified in B-C with NOD1/2 interactors identified by independent studies. *CCDC88A* (Girdin; white circle) emerges as a NOD2-specific interactor linked to tolerant ColAMs.

I. Heatmap of the correlation coefficient of normalized gene expression of *CCDC88A* with *NOD2* and *NOD1* across independent transcriptomic datasets of healthy and IBD tissues.

J. Bar graph of MDP/NOD2-induced NFκB activity observed during a functional genomic (siRNA-based) screen. The impact of depletion of iColAM genes and niColAM genes are presented. Interrupted line marks 75% enhancement relative to MDP-stimulated controls.

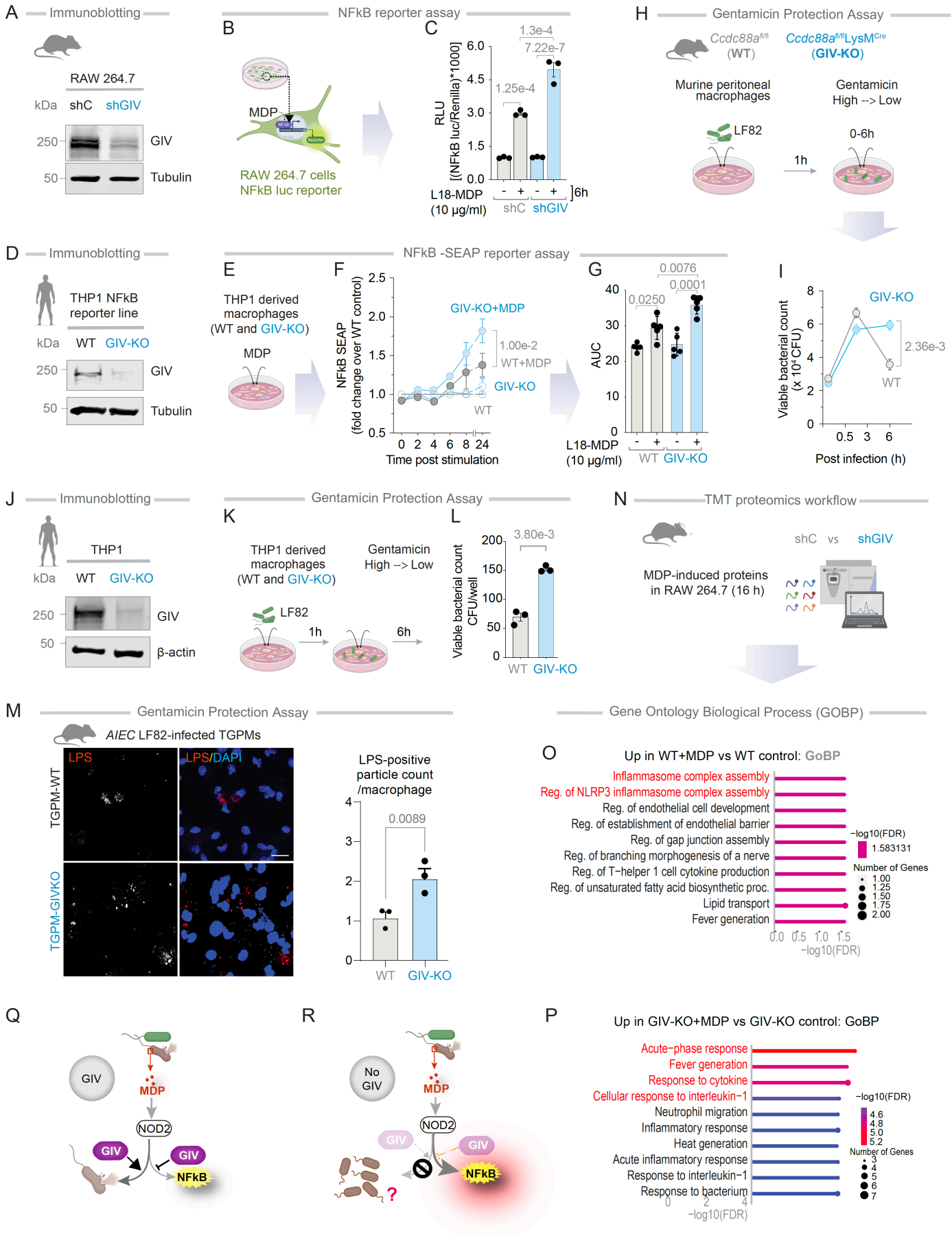

Figure 2. GIV dampens inflammation and promotes bacterial clearance in MDP-stimulated macrophages.

A. Immunoblot of control (shC) or GIV-depleted (shGIV) RAW 264.7 cells.

B-C. Workflow of the NFκB reporter assay in RAW 264.7 cells (B). Bar graphs display the fold change in NFκB activity (C).

D. Immunoblot of wild-type (WT; control) and GIV-knockout (GIV-KO) THP1-NFkB SEAP reporter cell line-derived macrophages.

E-G. Workflow of the NFκB reporter assay in CRISPR-depleted human THP-1 cells expressing an NFκB activity-tracking reporter (E). Line graphs (F) and AUC bar graphs (G) display the fold change in NFκB activity relative to WT control.

H-I. Workflow of the bacterial clearance assay (H). Line graphs (I) show the viable bacterial counts in the peritoneal macrophages.

J. Immunoblot of wild-type (WT; control) or GIV-knockout (GIV-KO) THP1 monocyte derived macrophage.

K-L. Workflow of the gentamicin protection assay in THP1 cells (K). Bar graphs (L) show the viable bacterial counts in the THP1 monocyte derived macrophage.

M. Immunofluorescence images display representative fields of TGPMs challenged with live *AIEC*-LF82 (MOI 1:30) for 1 h. Scale bar = 20 μM. Bar graphs display quantification of intracellular *AIEC*-LF82; n = 4-6.

N-P: Workflow for multiplexed proteomics analyses (N). Bar graphs (O and P) showing biological process as determined by gene ontology biological process analysis (Red, pathways cited in text).

Q-R. Schematics summarizing findings in cells with GIV (Q) and without GIV (R).

Statistics: All results are displayed as mean ± SEM (n = 3 biological replicates). Significance was tested using one-way ANOVA with Tukey's test (C and G), two-way ANOVA with Tukey's test (F and I), and 2-tailed Student's t-test (L and N). *p*-value ≤ 0.05 is considered as significant.

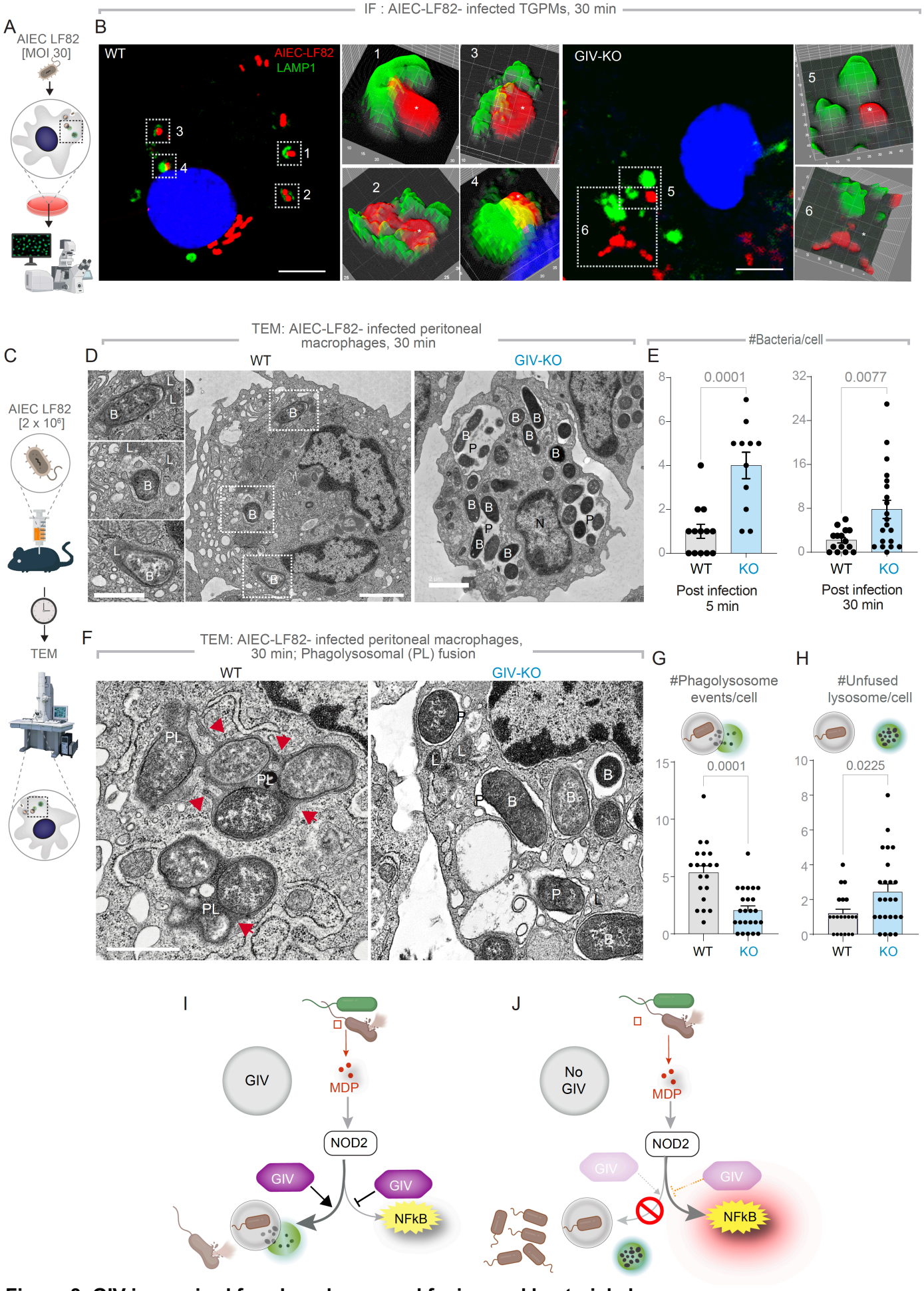

Figure 3. GIV is required for phagolysosomal fusion and bacterial clearance.

A-B. Workflow for immunofluorescence studies of *AIEC*-LF82-challenged TGPMs (A) and representative images (B) showing the proximity of *AIEC*-LF82 (red) to LAMP1-positive lysosomes (green). Insets show magnified, 3D-rendered versions of boxed regions, created using ImageJ. Scale bars = 5 μm

C. Workflow for TEM studies on infected peritoneal macrophages in D-H.

D. Representative TEM images showing bacterial abundance. Scale bar = 2 μm.

E. Bar graphs quantifying the number of bacteria per cell at 5- and 30-min post-infection.

F. High-magnification TEM images highlighting phagolysosomal (PL) fusion events (arrowheads).

G-H. Bar graphs display the number of events per cell (G) and number of unfused lysosomes per cell (H); n = 2 repeats. N=nucleus, P=phagosome, L=lysosome, PL=phagolysosome, B= bacteria AIEC-LF82.

I-J. Summary of findings in cells with (I) or without (J) GIV.

Statistics: All TEM quantifications are based on ~20-30 fields; n = 2 independent biological repeats. Results are presented as mean ± SEM. Significance was determined using 2-tailed Student's t-test; *p*-value ≤ 0.05 is considered as significant.

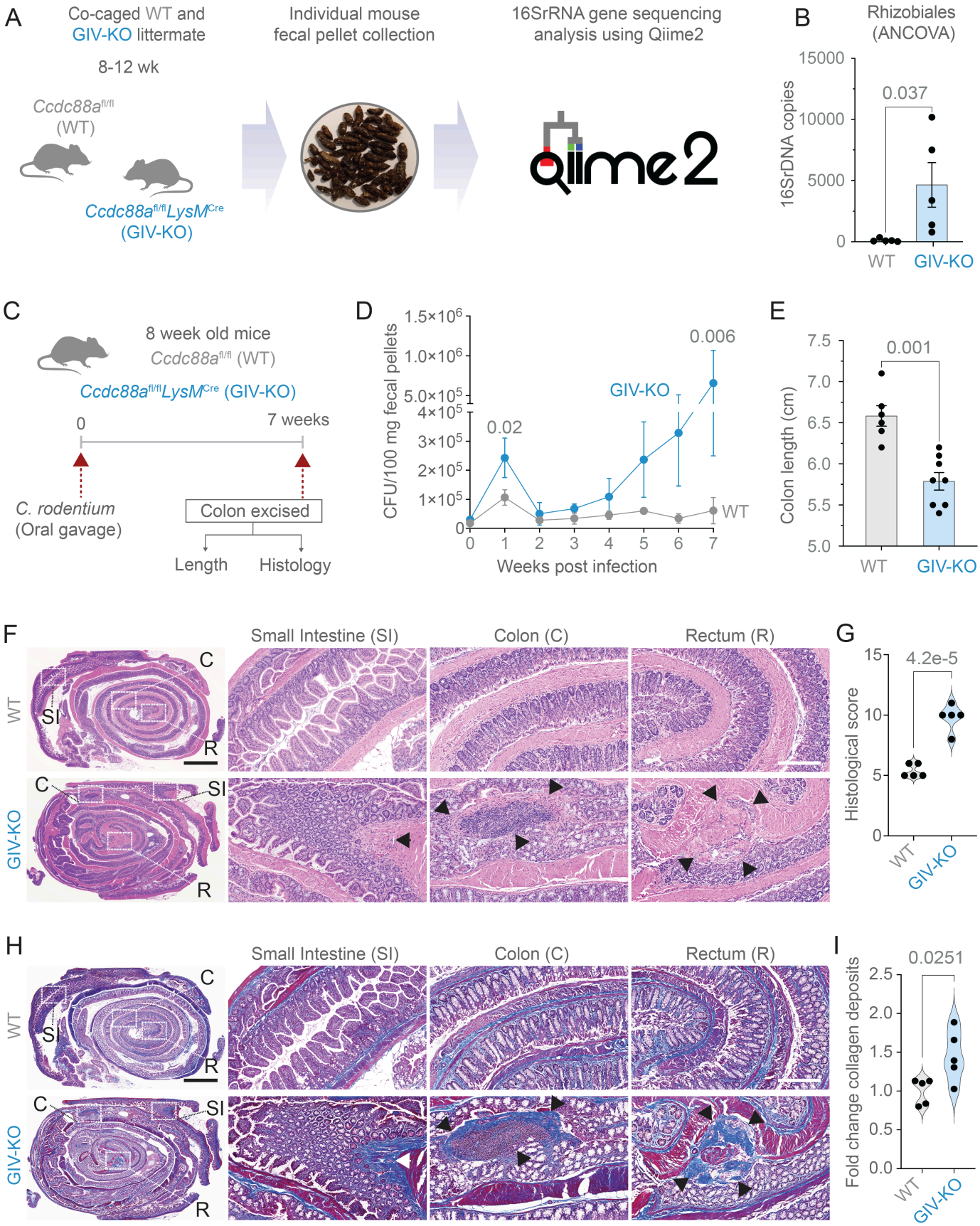

Figure 4. A mouse model of dysbiosis, impaired microbial clearance, patchy chronic transmural ileocolitis and fibrosis.

A-B. Schematic (A) and bar graph (B) display the process and outcome of a 16S fecal microbiome analysis at baseline in 10 wk-old myeloid-specific (*LysM*Cre) GIV-KO mice and their control littermates (WT). n = 5 mice in each group.

C-I. Panels describing the experimental design (**C**) and findings (**D-I**) in an infectious colitis model of GIV-KO and control littermates induced using *Citrobacter rodentium* (initially termed *Citrobacter freundii* biotype 4280 (88); strain name DBS100; 5 x 10^8 CFU/200ul/mouse. GIV-KO, n=8; WT, n=6. Findings are representative of two independent repeats. Line graphs (**D**) display the bacterial burden in fecal pellets over a 7 wk period after the initial oral gavage. Bar graph (**E**) displays the differences in colon length. H&E (**F**) or trichrome (**H**)-stained images representative of Swiss rolls of the entire intestinal tract are shown. Scale bar = 2.5 mm. Magnified fields of the rectum (R), colon (C) and small intestine (SI) of the corresponding boxed regions are shown. Scale bar = 250 μm. Arrows show regions of transmural inflammation/crypt distortion, immune infiltrates (in F) correspond also to transmural fibrosis (in H). Segments in between these patches appear normal. Bar graphs show the histology index (89) (**G**; based on submucosal inflammation, percent area involved, inflammatory infiltrates in LP and crypt hyperplasia and the degree of fibrosis (**I**), as assessed by H&E and trichrome staining on n = 5 WT and 5 GIV-KO mice.

Statistics: All results are displayed as mean ± SEM. Significance was tested using 2-tailed Student's t-test. Only significant *p*-values ($p \leq 0.05$) are shown. *p*-value ≤ 0.05 is considered as significant.

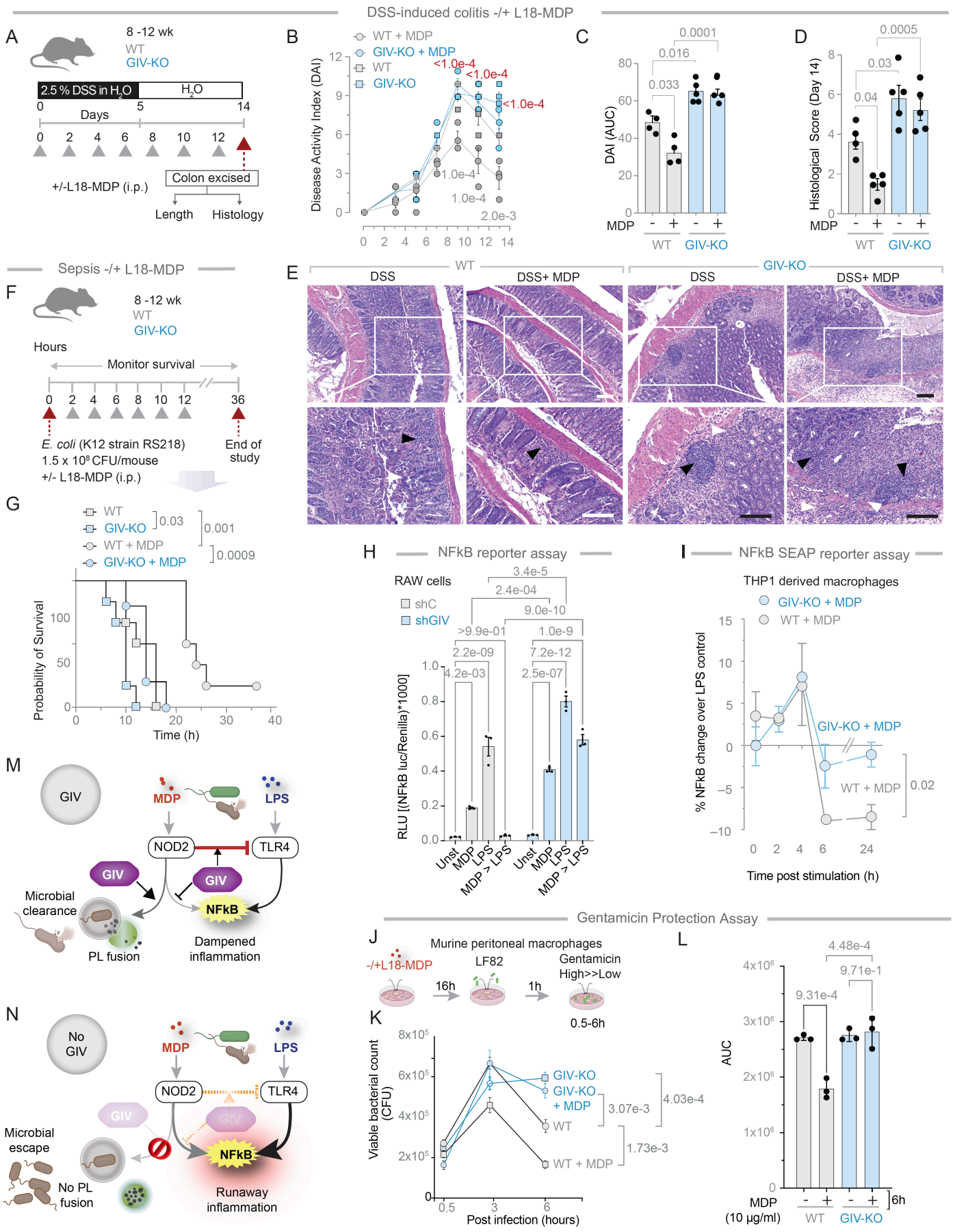

Figure 5. **GIV-KO mice and cells are insensitive to the protective actions of MDP/NOD2 signals**. **A-E**. Schematic (A) displays the study design for DSS-induced colitis. GIV-KO, n=5; WT, n=5. Findings are representative of two independent repeats. Grey arrowheads denote the alternate day administration of

muramyl dipeptide (MDP) (100μg/mouse/day). Line graphs (B) display disease activity index (DAI), calculated for the days 3, 5, 7, 9, 11 and 13 after DSS administration, which accounts for stool consistency (0-4), rectal bleeding (0-4), and weight loss (0-4). *p* value in gray and red color text represents significance WT vs WT+MDP and WT+MDP vs GIVKO+MDP respectively. Bar graphs (C) represent the data in B as area under the curves (AUC) in B. Bar graphs (D) display the histological score on day 14, as assessed by a well-accepted methodology (90) of analyzing H&E-stained distal colons from the mice. Representative images are displayed in E. Arrowheads point to regions of crypt destruction and/or inflammatory infiltrates. Scale bar = 200 μm.

F-G. Schematic (F) displays the sepsis study design in which 8 mice in each group were treated with E coli and MDP simultaneously, followed by periodic checks for death (arrowheads). Kaplan-Meier plot (G) displays the % of cohort that survived at those time points. GIV-KO, n=8; WT, n=8. Findings are representative of two independent repeats.

H. Bar graphs display the impact of MDP (10 μg/ml) priming on LPS (100 ng/ml)-induced NFκB activity.

I. Line graphs display percent change in LPS (100 ng/ml)-induced NFκB activity in WT and GIV-KO cells primed with MDP (10 μg/ml).

J-L. Schematic (J) displays the experimental setup for bacterial clearance. Line graphs (K) show the viable bacterial counts in the macrophages. Bar graphs (L) represent the data in (K) as the area under the curve (AUC).

M-N. Schematic summarizing findings in cells with (M) or without (N) GIV.

Statistics: All results are displayed as mean ± SEM. Significance was tested using one-way ANOVA with Tukey's test C, D, H and L), two-way ANOVA with Tukey's test (B, I and K) and Mantel-Cox log rank test (G). *p*-value ≤ 0.05 is considered as significant.

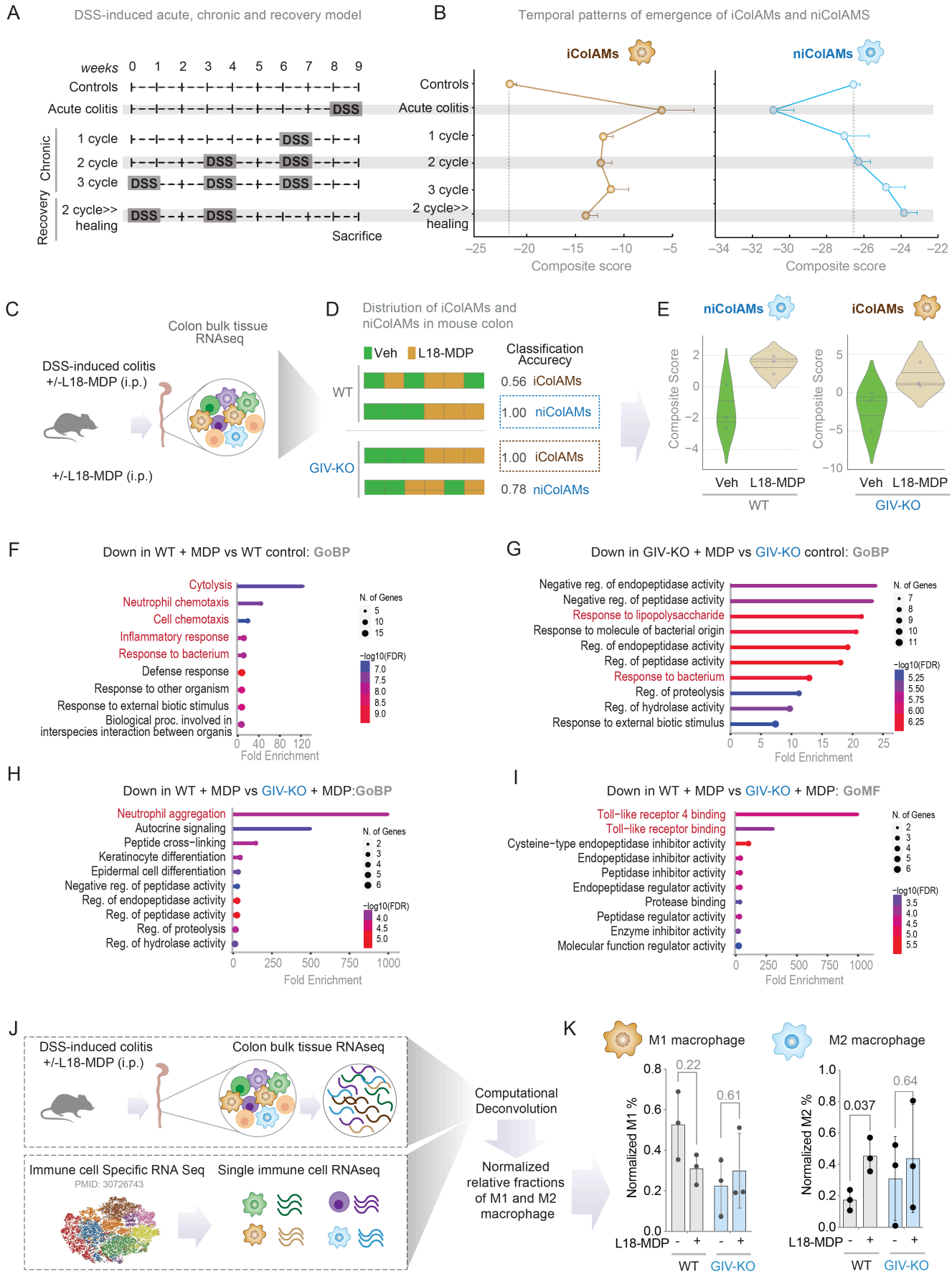

Figure 6. GIV is required for the emergence of healing niColAMs in MDP-treated WT mice.

A. Study design of DSS-induced acute, chronic and recovery in mouse models of colitis (C57/BL6; all WT).

B. Line graphs display the temporal patterns of the emergence of iColAMs and niColAMs in the colon samples in A. The grey dotted line indicates the composite scores of iColAM and niColAM genes in the control mice.
C-E. Study design (C) for DSS-induced colitis in WT vs. GIV mice (n=3 each). See also **Figure 5A-E** for the detailed study design and disease pathology. Bar plots (D) show the classification accuracy of composite scores derived from iColAM and niColAM gene signatures in DSS-challenged mouse samples, comparing with or without L18-MDP treatment groups. Classification strength within each cohort is measured using ROC-AUC analyses. Violin plots (E) show composite scores for niColAMs (for blue border in D) in WT and iColAMs (for brown border in D) in GIV-KO mice, treated with or without L18-MDP.
F-G. Gene Ontology Biological Process (Go-BP) pathway enrichment analyses of genes downregulated in WT (F) or GIV-KO (G) mice treated with L18-MDP compared to their respective untreated controls.
H-I. GoBP (H) and Go Molecular Function (GO MF; I) analyses of genes downregulated in L18-MDP-treated WT vs. GIV-KO samples.
J-K. Schematic (J) of bulk RNA sequencing *in silico* deconvolution analysis of distal colons from DSS-treated mice in C. Bar plots (K) show normalized percentage abundances of M1 and M2 macrophages in WT and GIV-KO mice, with and without MDP treatment.
Statistics: *p*-values were calculated using an unpaired multiple t-test (K). *p*-value ≤ 0.05 is considered as significant.

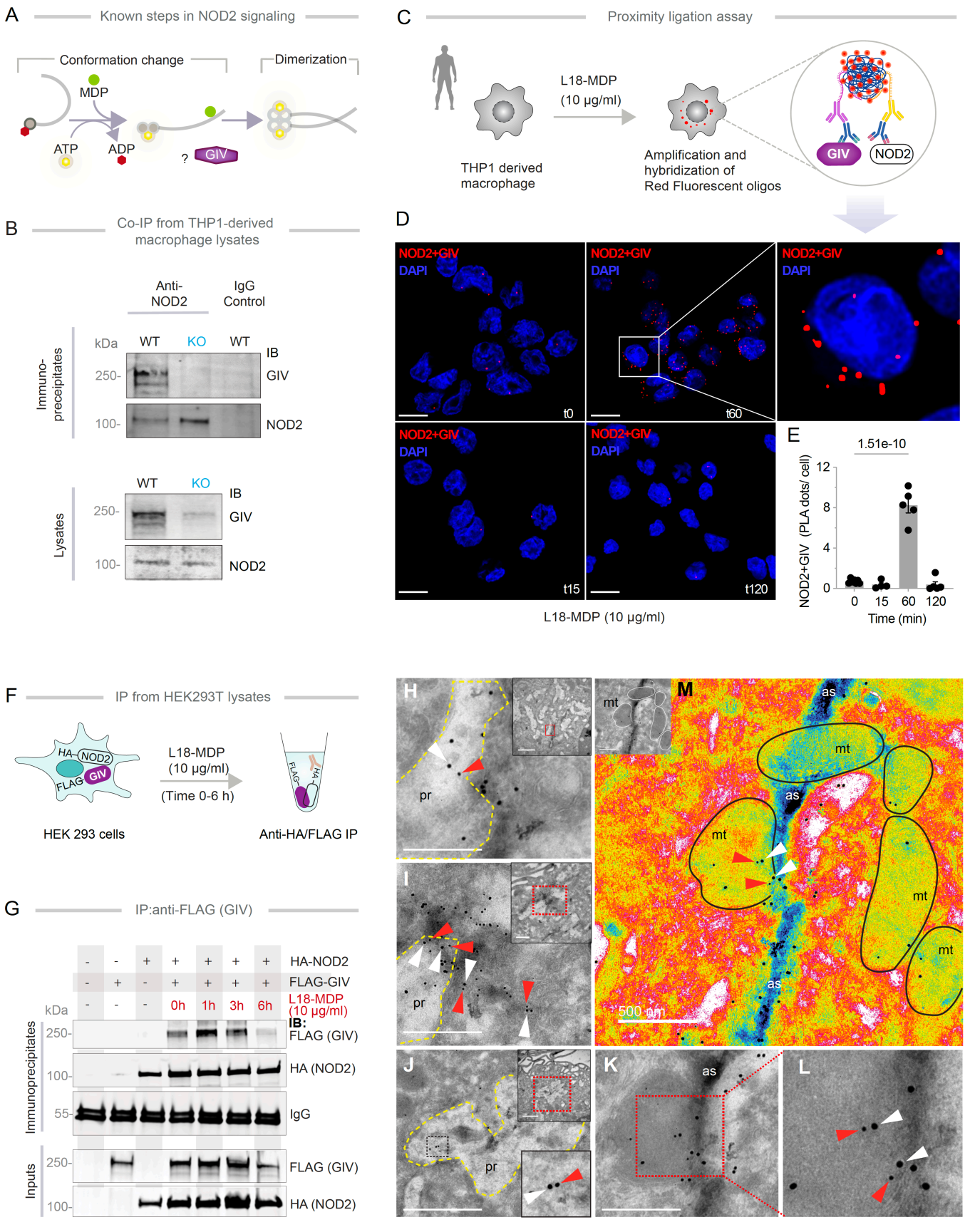

Figure 7. NOD2 and GIV colocalize and interact in cells

A. Schematic displays key steps in MDP-induced NOD2 signaling. In resting cells, ADP-bound inactive NOD2 exists in an autoinhibited conformation. In resting cells, ADP-bound NOD2 is autoinhibited. Upon ligand

(MDP) stimulation, ADP is exchanged for ATP, stabilizing ligand binding, inducing conformational change and "opening" of the LRR module, followed by NOD2 dimerization and assembly of signaling complexes.

B. Immunoprecipitation of full-length endogenous NOD2 from THP1-derived macrophage lysates. Immune complexes were analyzed for bound GIV by immunoblotting (IB); input lysates were probed for NOD2 and GIV.

C-E. Study design of proximity ligation assay (PLA; **C**). Representative confocal images (**D**) show colocalization of GIV and NOD2 in THP1 derived macrophages challenged with MDP for 0-120 min. Scale bar = 10 μm. Quantification (**E**) from ~20-30 randomly imaged fields; n = 4-5 repeats. *p* value determined by one-way ANOVA, followed by Tukey's test for multiple comparisons and indicated with *p*-values shown above bars. *p*-value ≤ 0.05 is considered as significant.

F-G. Schematic depicts study design of immunoprecipitation from lysates of HEK293T cells (**F**). HA-tagged NOD2 was immunoprecipitated with anti-HA mAb from equal aliquots of lysates of HEK293T cells co-expressing GIV-FLAG and HA-NOD2, stimulated (+) or not (-) with MDP for indicated time points. Immunoprecipitated (IP) complexes and input lysates were analyzed for NOD2 and GIV by immunoblotting (IB) (**G**).

H-M. TEM micrographs display representative images of colocalization of GIV (white arrowheads; 18 nm gold particles) and NOD2 (red arrowheads; 12 nm gold particles) on TGPMs challenged with live AIEC-LF82 (MOI 1:30) for 1 h. NOD2 colocalization within particle-rich cytoplasmic structures (pr), with membrane-associated GIV on actin strands (as, Pseudo-colored blue) and swollen mitochondria (mt, outlined in black) with degraded cristae in **M** and. Scale bar = 500 nM.

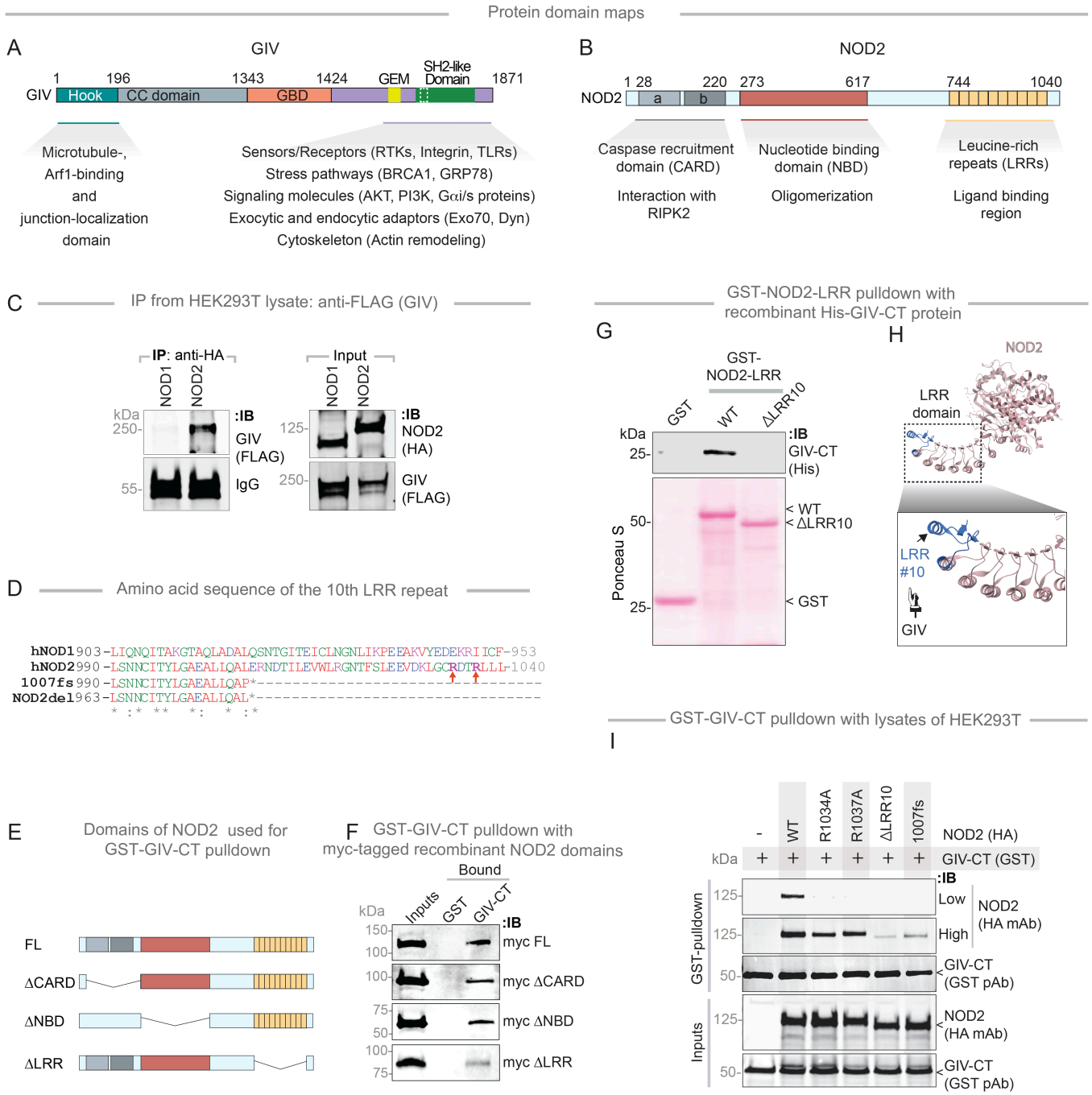

Figure 8. The NOD2(LRR)•GIV(C-term) interaction is direct and ligand-dependent

A-B. Schematic depicts the domain maps of (A) GIV and (B) NOD2 and highlights established functions and interactions facilitated by the domains.

C. HA-tagged NOD1/2 proteins were immunoprecipitated from equal aliquots of lysates of HEK293T cells co-transfected with GIV and either NOD1 or NOD2 using anti-HA mAb. Immunoprecipitated (IP) complexes and input lysates were analyzed for NOD1/2 and GIV by immunoblotting (IB).

D. An alignment of the amino acid sequence of the 10th LRR repeat of human hNOD1, hNOD2, the CD-risk associated NOD2 variant (NOD2-*1007fs*) and the deletion mutant generated in this work (NOD2-del) is shown. Residues mutated in this study to evaluate potential participating residues in the NOD2•GIV interaction are highlighted.

E-F. Schematics indicate the domains of NOD2 that were used to generate myc-tagged recombinant proteins for use in GST-pulldown assays in **E**. Equal aliquots of recombinant myc-NOD2 domains (~3 μg; input, **F**) were used in pulldown assays with immobilized GST and GST-GIV in **F**. Myc-tagged NOD2 was visualized by immunoblot (IB) using anti-myc antibody.

G-H. GST-pulldown assay (G) was carried out using GST NOD2-LRR proteins as indicated and bound His-GIV-CT is assessed. Schematic (H) highlights the terminal LRR repeat (blue) of NOD2 which binds GIV.

I. GST-GIV-CT was pulled down using Glutathione beads from equal aliquots of lysates of HEK293T lysates co-expressing GST-GIV-CT (aa 1660-1870; mammalian p-CEFL vector) and either WT or HA-NOD2 mutants predicted to disrupt NOD•GIV binding. Immunoprecipitated (IP) complexes and input lysates were analyzed for NOD2 and GIV-CT by immunoblotting (IB), using anti-HA (NOD2) and anti-GST (GIV-CT) antibodies.

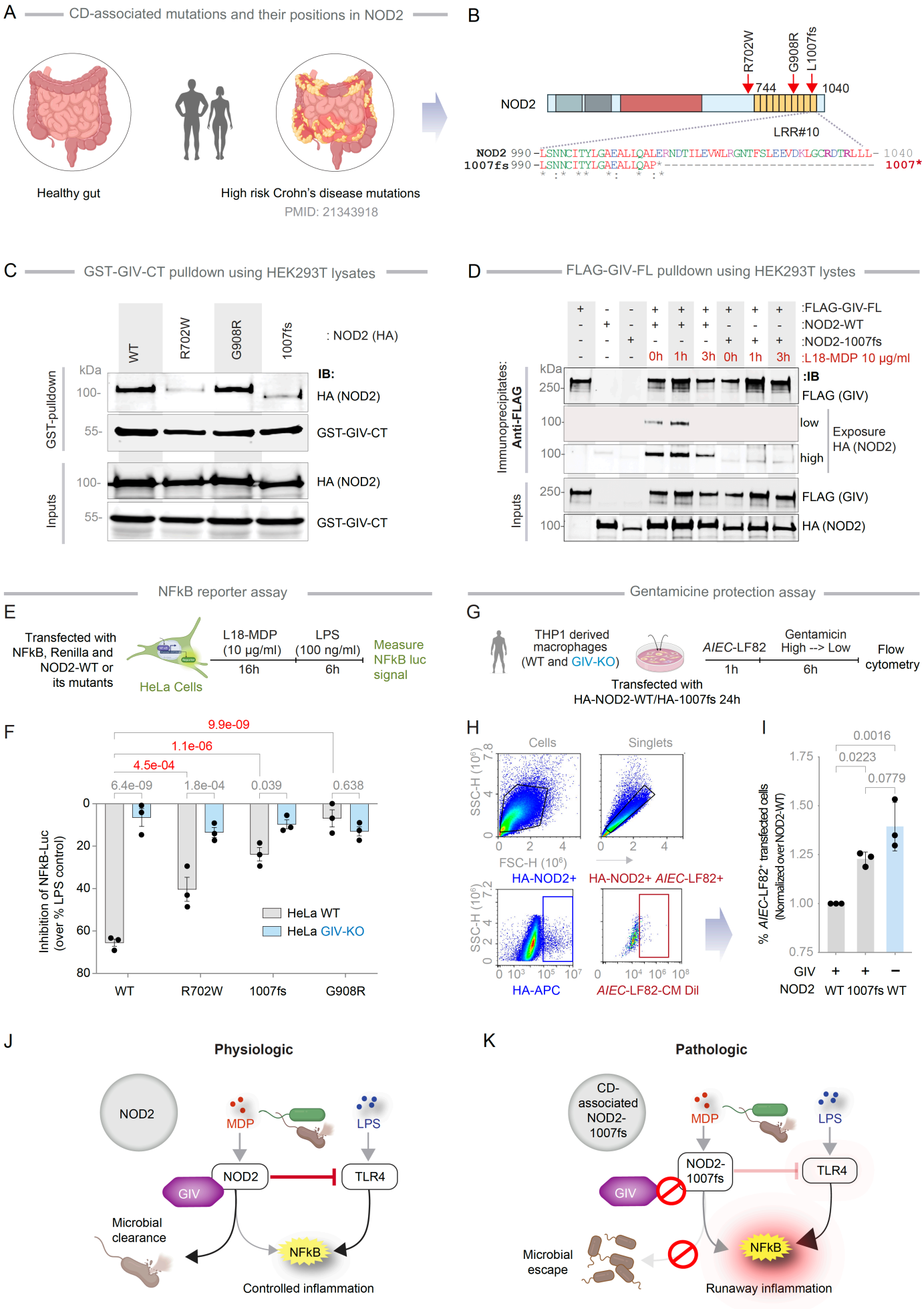

Figure 9: Characterization of the NOD2•GIV interface exploiting CD-associated NOD2 mutants.

A-B. Schematic shows (A) CD-associated mutations and their positions in NOD2, depicts as a domain map and an alignment (B) of the amino acid sequence of the 10th LRR repeat of human NOD2 and the CD-risk associated NOD2 variant (NOD2-*1007fs*) are shown. Residues mutated in this study to evaluate potential participating residues in the NOD2•GIV interaction are highlighted.

C. GST-GIV-CT was pulled down using Glutathione beads from equal aliquots of lysates of HEK293T co-expressing GST-GIV-CT (aa 1660-1870; mammalian p-CEFL vector) and wild-type (WT) or 3 indicated CD-risk associated variants of HA-NOD2. Bound NOD2 proteins and similar expression of GIV-CT was assessed by immunoblotting (IB) using anti-HA (NOD2) and anti-GST (GIV-CT) antibodies.

D. FLAG-tagged GIV was immunoprecipitated with anti-FLAG mAb from equal aliquots of lysates of HEK293T cells expressing GIV-FLAG and either wild-type (WT) or *1007fs* variant of HA-NOD2, stimulated (+) or not (-) with MDP for the indicated time points. Immunoprecipitated (IP) complexes and input lysates were analyzed for NOD2 and GIV by immunoblotting (IB), using anti-HA (NOD2) and anti-FLAG (GIV-CT) antibodies.

E-F. Schematic (E) outlining the workflow for assessing NFκB activity. Bar graphs (F) display NFκB reporter assay in HeLa cells. Cells were pre-incubated with MDP (10 μg/ml) and then stimulated with LPS (100 ng/ml) and % change of NFκB activity was detected using dual cell reporter assay.

G-I. Schematic (G) outlining the workflow for assessing bacterial clearance via flow cytometry. The flow cytometry panel (H) detects CM-DiI labeled *AIEC*-LF82 bacteria (MOI 1:30) in THP1-derived macrophages transfected with HA-NOD2-WT or 1007fs mutant. Bar graphs (I) display *AIEC*-LF82 bacterial load normalized to NOD2-WT. Statistical significance was assessed using one-way ANOVA followed by Tukey's multiple comparison test; p-value ≤ 0.05 is considered significant.

J-K. Schematic summarizing key findings in this work. Magenta colored solid and interrupted lines indicate the GIV-dependent impact on NOD2 that were interrogated in this work. (**J**) In physiology, bacterial sensing and signaling by NOD2 requires GIV to limit inflammation. (**K**) In pathology, dysregulated inflammation results when either wild-type NOD2 cannot bind GIV (e.g., GIV is low/absent) or when CD-risk associated *1007fs* variant cannot bind GIV.

Statistics: p-values were calculated using one-way ANOVA with Tukey's test (I) and two-way ANOVA with Tukey's test (F) and indicated with p-values shown above bars. p-value ≤ 0.05 is considered as significant.

REFERENCES

1. Yang W, and Cong Y. Gut microbiota-derived metabolites in the regulation of host immune responses and immune-related inflammatory diseases. *Cell Mol Immunol.* 2021;18(4):866-77.
2. Katkar G, and Ghosh P. Macrophage states: there's a method in the madness. *Trends Immunol.* 2023;44(12):954-64.
3. Ghosh P, et al. Machine learning identifies signatures of macrophage reactivity and tolerance that predict disease outcomes. *EBioMedicine.* 2023;94:104719.
4. Marks DJ. Defective innate immunity in inflammatory bowel disease: a Crohn's disease exclusivity? *Curr Opin Gastroenterol.* 2011;27(4):328-34.
5. Davies JM, and Abreu MT. The innate immune system and inflammatory bowel disease. *Scand J Gastroenterol.* 2015;50(1):24-33.
6. Gordon S, and Plüddemann A. Tissue macrophages: heterogeneity and functions. *BMC Biol.* 2017;15(1):53.
7. Sahoo D, et al. Artificial intelligence guided discovery of a barrier-protective therapy in inflammatory bowel disease. *Nat Commun.* 2021;12(1):4246.
8. Sahoo D, et al. AI-guided discovery of the invariant host response to viral pandemics. *EBioMedicine.* 2021;68:103390.
9. Pandya R, et al. A machine learning classifier using 33 host immune response mRNAs accurately distinguishes viral and non-viral acute respiratory illnesses in nasal swab samples. *Genome Med.* 2023;15(1):64.
10. Zhang Z, et al. Deciphering the crosstalk of immune dysregulation between COVID-19 and idiopathic inflammatory myopathy. *Front Immunol.* 2023;14:1197493.
11. Dalerba P, et al. CDX2 as a Prognostic Biomarker in Stage II and Stage III Colon Cancer. *N Engl J Med.* 2016;374(3):211-22.
12. Ghosh P, et al. AI-assisted discovery of an ethnicity-influenced driver of cell transformation in esophageal and gastroesophageal junction adenocarcinomas. *JCI Insight.* 2022;7(18).
13. Ashton JJ, et al. Deleterious Genetic Variation Across the NOD Signaling Pathway Is Associated With Reduced NFKB Signaling Transcription and Upregulation of Alternative Inflammatory Transcripts in Pediatric Inflammatory Bowel Disease. *Inflamm Bowel Dis.* 2022.
14. Watanabe T, et al. NOD2 is a negative regulator of Toll-like receptor 2-mediated T helper type 1 responses. *Nat Immunol.* 2004;5(8):800-8.
15. Watanabe T, et al. Muramyl dipeptide activation of nucleotide-binding oligomerization domain 2 protects mice from experimental colitis. *J Clin Invest.* 2008;118(2):545-59.
16. Watanabe T, et al. NOD2 regulation of Toll-like receptor responses and the pathogenesis of Crohn's disease. *Gut.* 2005;54(11):1515-8.
17. Watanabe T, et al. NOD2 downregulates colonic inflammation by IRF4-mediated inhibition of K63-linked polyubiquitination of RICK and TRAF6. *Mucosal Immunol.* 2014;7(6):1312-25.
18. Negroni A, et al. NOD2 and inflammation: current insights. *J Inflamm Res.* 2018;11:49-60.
19. Ghosh P, et al. The GAPs, GEFs, GDIs and...now, GEMs: New kids on the heterotrimeric G protein signaling block. *Cell Cycle.* 2017;16(7):607-12.
20. Garcia-Marcos M, et al. GIV is a nonreceptor GEF for G alpha i with a unique motif that regulates Akt signaling. *Proc Natl Acad Sci U S A.* 2009;106(9):3178-83.
21. Gupta V, et al. GIV/Girdin activates Gαi and inhibits Gαs via the same motif. *Proc Natl Acad Sci U S A.* 2016;113(39):E5721-30.
22. Swanson L, et al. TLR4 signaling and macrophage inflammatory responses are dampened by GIV/Girdin. *Proc Natl Acad Sci U S A.* 2020;117(43):26895-906.
23. Ghosh P, et al. The stress polarity signaling (SPS) pathway serves as a marker and a target in the leaky gut barrier: implications in aging and cancer. *Life Sci Alliance.* 2020;3(3).
24. Peters LA, et al. A functional genomics predictive network model identifies regulators of inflammatory bowel disease. *Nat Genet.* 2017;49(10):1437-49.
25. Breynaert C, et al. Unique gene expression and MR T2 relaxometry patterns define chronic murine dextran sodium sulphate colitis as a model for connective tissue changes in human Crohn's disease. *PLoS One.* 2013;8(7):e68876.
26. Jostins L, et al. Host-microbe interactions have shaped the genetic architecture of inflammatory bowel disease. *Nature.* 2012;491(7422):119-24.
27. Liu JZ, et al. Association analyses identify 38 susceptibility loci for inflammatory bowel disease and highlight shared genetic risk across populations. *Nat Genet.* 2015;47(9):979-86.

28. Philpott DJ, et al. NOD proteins: regulators of inflammation in health and disease. *Nat Rev Immunol.* 2014;14(1):9-23.
29. Caruso R, et al. NOD1 and NOD2: signaling, host defense, and inflammatory disease. *Immunity.* 2014;41(6):898-908.
30. McCarthy JV, et al. RIP2 is a novel NF-kappaB-activating and cell death-inducing kinase. *J Biol Chem.* 1998;273(27):16968-75.
31. Nachbur U, et al. A RIPK2 inhibitor delays NOD signalling events yet prevents inflammatory cytokine production. *Nat Commun.* 2015;6:6442.
32. Lesage S, et al. CARD15/NOD2 mutational analysis and genotype-phenotype correlation in 612 patients with inflammatory bowel disease. *Am J Hum Genet.* 2002;70(4):845-57.
33. Kufer TA, et al. Innate immune sensing of microbes by Nod proteins. *Ann N Y Acad Sci.* 2006;1072:19-27.
34. Rescigno M, and Nieuwenhuis EE. The role of altered microbial signaling via mutant NODs in intestinal inflammation. *Curr Opin Gastroenterol.* 2007;23(1):21-6.
35. Vignal C, et al. How NOD2 mutations predispose to Crohn's disease? *Microbes Infect.* 2007;9(5):658-63.
36. Nelson A, et al. The Impact of NOD2 Genetic Variants on the Gut Mycobiota in Crohn's Disease Patients in Remission and in Individuals Without Gastrointestinal Inflammation. *J Crohns Colitis.* 2021;15(5):800-12.
37. Lu Y, et al. Palmitoylation of NOD1 and NOD2 is required for bacterial sensing. *Science.* 2019;366(6464):460-7.
38. Warner N, et al. A genome-wide siRNA screen reveals positive and negative regulators of the NOD2 and NF-κB signaling pathways. *Sci Signal.* 2013;6(258):rs3.
39. Graham DB, and Xavier RJ. Pathway paradigms revealed from the genetics of inflammatory bowel disease. *Nature.* 2020;578(7796):527-39.
40. Hugot JP, et al. Association of NOD2 leucine-rich repeat variants with susceptibility to Crohn's disease. *Nature.* 2001;411(6837):599-603.
41. Ogura Y, et al. A frameshift mutation in NOD2 associated with susceptibility to Crohn's disease. *Nature.* 2001;411(6837):603-6.
42. Eckmann L, and Karin M. NOD2 and Crohn's disease: loss or gain of function? *Immunity.* 2005;22(6):661-7.
43. Rogler G, et al. Nuclear factor kappaB is activated in macrophages and epithelial cells of inflamed intestinal mucosa. *Gastroenterology.* 1998;115(2):357-69.
44. Maeda S, et al. Nod2 mutation in Crohn's disease potentiates NF-kappaB activity and IL-1beta processing. *Science.* 2005;307(5710):734-8.
45. Economou M, et al. Differential effects of NOD2 variants on Crohn's disease risk and phenotype in diverse populations: a metaanalysis. *Am J Gastroenterol.* 2004;99(12):2393-404.
46. Freire P, et al. NOD2 gene mutations in ulcerative colitis: useless or misunderstood? *Int J Colorectal Dis.* 2014;29(6):653-61.
47. Damgaard RB, et al. The ubiquitin ligase XIAP recruits LUBAC for NOD2 signaling in inflammation and innate immunity. *Mol Cell.* 2012;46(6):746-58.
48. Hao H, et al. Lipoxin A4 suppresses lipopolysaccharide-induced hela cell proliferation and migration via NF-κB pathway. *Inflammation.* 2015;38(1):400-8.
49. Darfeuille-Michaud A, et al. High prevalence of adherent-invasive Escherichia coli associated with ileal mucosa in Crohn's disease. *Gastroenterology.* 2004;127(2):412-21.
50. Herskovits AA, et al. Bacterial ligands generated in a phagosome are targets of the cytosolic innate immune system. *PLoS Pathog.* 2007;3(3):e51.
51. Kaakoush NO, et al. Microbial dysbiosis in pediatric patients with Crohn's disease. *J Clin Microbiol.* 2012;50(10):3258-66.
52. Zhang K, et al. Macrophage polarization in inflammatory bowel disease. *Cell Commun Signal.* 2023;21(1):367.
53. Angriman I, et al. Innate Immunity Activation in Newly Diagnosed Ileocolonic Crohn's Disease: A Cohort Study. *Dis Colon Rectum.* 2024;67(5):681-92.
54. Fu Y, et al. PLXDC1 serves as a potential prognostic marker and involves in malignant progression and macrophage polarization in colon cancer. *J Biochem Mol Toxicol.* 2024;38(10):e23832.
55. Cobb JP, et al. Muramyl dipeptide protects decomplemented mice from surgically-induced infection. *Int J Immunopharmacol.* 1986;8(7):799-803.

56. Matsumoto K, et al. Stimulation of nonspecific host resistance to infection induced by muramyldipeptides. *Microbiol Immunol.* 1981;25(10):1047-58.
57. Wardowska A, et al. Analogues of muramyl dipeptide (MDP) and tuftsin limit infection and inflammation in murine model of sepsis. *Vaccine.* 2009;27(3):369-74.
58. Katkar GD, et al. Artificial Intelligence-rationalized balanced PPARα/γ dual agonism resets the dysregulated macrophage processes in inflammatory bowel disease. *bioRxiv.* 2021:2021.07.18.452807.
59. Whittem CG, et al. Murine Colitis modeling using Dextran Sulfate Sodium (DSS). *J Vis Exp.* 2010(35).
60. Kim H, et al. A novel crosstalk between TLR4- and NOD2-mediated signaling in the regulation of intestinal inflammation. *Sci Rep.* 2015;5:12018.
61. Wang J, et al. Cancer-derived immunoglobulin G promotes LPS-induced proinflammatory cytokine production via binding to TLR4 in cervical cancer cells. *Oncotarget.* 2014;5(20):9727-43.
62. Jiang N, et al. Toll-like receptor 4 promotes proliferation and apoptosis resistance in human papillomavirus-related cervical cancer cells through the Toll-like receptor 4/nuclear factor-κB pathway. *Tumour Biol.* 2017;39(6):1010428317710586.
63. Manna SK, and Aggarwal BB. Lipopolysaccharide inhibits TNF-induced apoptosis: role of nuclear factor-kappaB activation and reactive oxygen intermediates. *J Immunol.* 1999;162(3):1510-8.
64. Sulistyowati E, et al. Exogenous Heat Shock Cognate Protein 70 Suppresses LPS-Induced Inflammation by Down-Regulating NF-κB through MAPK and MMP-2/-9 Pathways in Macrophages. *Molecules.* 2018;23(9).
65. Xiong D, et al. Salmonella Coiled-Coil- and TIR-Containing TcpS Evades the Innate Immune System and Subdues Inflammation. *Cell Rep.* 2019;28(3):804-18.e7.
66. Pridmore AC, et al. Activation of toll-like receptor 2 (TLR2) and TLR4/MD2 by Neisseria is independent of capsule and lipooligosaccharide (LOS) sialylation but varies widely among LOS from different strains. *Infect Immun.* 2003;71(7):3901-8.
67. Gong Q, et al. Structural basis of RIP2 activation and signaling. *Nat Commun.* 2018;9(1):4993.
68. Ellwanger K, et al. XIAP controls RIPK2 signaling by preventing its deposition in speck-like structures. *Life Sci Alliance.* 2019;2(4).
69. Solcia E, et al. Particle-rich cytoplasmic structure (PaCS): identification, natural history, role in cell biology and pathology. *Biomolecules.* 2014;4(3):848-61.
70. Maekawa S, et al. Crystal structure of NOD2 and its implications in human disease. *Nat Commun.* 2016;7:11813.
71. Adler J, et al. The prognostic power of the NOD2 genotype for complicated Crohn's disease: a meta-analysis. *Am J Gastroenterol.* 2011;106(4):699-712.
72. Boyle JP, et al. Comparative Genomic and Sequence Analysis Provides Insight into the Molecular Functionality of NOD1 and NOD2. *Front Immunol.* 2013;4:317.
73. Vijayrajratnam S, et al. Understanding the molecular differential recognition of muramyl peptide ligands by LRR domains of human NOD receptors. *Biochem J.* 2017;474(16):2691-711.
74. Zhou H, et al. Activation of Both TLR and NOD Signaling Confers Host Innate Immunity-Mediated Protection Against Microbial Infection. *Front Immunol.* 2018;9:3082.
75. Boyle JP, et al. Insights into the molecular basis of the NOD2 signalling pathway. *Open Biol.* 2014;4(12).
76. Kim D, et al. Nod2-mediated recognition of the microbiota is critical for mucosal adjuvant activity of cholera toxin. *Nat Med.* 2016;22(5):524-30.
77. Gerlo S, et al. Cyclic AMP: a selective modulator of NF-κB action. *Cell Mol Life Sci.* 2011;68(23):3823-41.
78. Park JM, et al. Signaling pathways and genes that inhibit pathogen-induced macrophage apoptosis--CREB and NF-kappaB as key regulators. *Immunity.* 2005;23(3):319-29.
79. Peters-Golden M. Putting on the brakes: cyclic AMP as a multipronged controller of macrophage function. *Sci Signal.* 2009;2(75):pe37.
80. Kalamidas SA, et al. cAMP synthesis and degradation by phagosomes regulate actin assembly and fusion events: consequences for mycobacteria. *J Cell Sci.* 2006;119(Pt 17):3686-94.
81. Ghosh P, and Mullick M. Building unconventional G protein-coupled receptors, one block at a time. *Trends Pharmacol Sci.* 2021;42(7):514-7.
82. Heerasing N, and Kennedy NA. Interaction Between NOD2 and Smoking in the Pathogenesis of Crohn's Disease. *EBioMedicine.* 2017;21:49-50.
83. Lécine P, et al. The NOD2-RICK complex signals from the plasma membrane. *J Biol Chem.* 2007;282(20):15197-207.

84. McDonald C, et al. A role for Erbin in the regulation of Nod2-dependent NF-kappaB signaling. *J Biol Chem.* 2005;280(48):40301-9.
85. Pizarro TT, et al. SAMP1/YitFc mouse strain: a spontaneous model of Crohn's disease-like ileitis. *Inflamm Bowel Dis.* 2011;17(12):2566-84.
86. Okai N, et al. Crosstalk between NOD2 and TLR2 suppresses the development of TLR2-mediated experimental colitis. *J Clin Biochem Nutr.* 2024;74(2):146-53.
87. Perez-Riverol Y, et al. The PRIDE database resources in 2022: a hub for mass spectrometry-based proteomics evidences. *Nucleic Acids Res.* 2022;50(D1):D543-d52.
88. Newman JV, et al. Citrobacter rodentium espB is necessary for signal transduction and for infection of laboratory mice. *Infect Immun.* 1999;67(11):6019-25.
89. Bouladoux N, et al. The Mouse Model of Infection with Citrobacter rodentium. *Curr Protoc Immunol.* 2017;119:19.5.1-.5.25.
90. Kim JJ, et al. Investigating intestinal inflammation in DSS-induced model of IBD. *J Vis Exp.* 2012(60).